Spatiotemporal disease suitability prediction for Oropouche virus and the role of vectors across the Americas

Jenicca Poongavanan[1], Marcel Dunaiski[2], Graeme D'or[1], Moritz U.G. Kraemer[3,4], Marta Giovanetti[5,6,7], Ahyoung Lim[8,9], Oliver J. Brady[8,9], Cheryl Baxter[1], Vagner Fonseca[1,10], Luiz Alcantara[7], Tulio de Oliveira[1,11], Houriiyah Tegally[1*]

[1]Centre for Epidemic Response and Innovation (CERI), School for Data Science and Computational Thinking, Stellenbosch University, Stellenbosch 7600, South Africa.

[2]Computer Science Division, Department of Mathematical Sciences, Stellenbosch University, Stellenbosch, South Africa

[3]Pandemic Sciences Institute, University of Oxford, UK

[4]Department of Biology, University of Oxford, Oxford,UK

[5]Department of Sciences and Technologies for Sustainable Development and One Health, Università Campus Bio-Medico di Roma, Rome, Italy.

[6]Oswaldo Cruz Institute, Oswaldo Cruz Foundation, Rio de Janeiro, Brazil.

[7]René Rachou Institute, Oswaldo Cruz Foundation, Belo Horizonte.

[8]Department of Infectious Disease Epidemiology and Dynamics, London School of Hygiene and Tropical Medicine, London, United Kingdom

[9]Centre for the Mathematical Modelling of Infectious Diseases, London School of Hygiene and Tropical Medicine, London, United Kingdom

[10]Department of Exact and Earth Sciences, University of the State of Bahia, Salvador, Brazil

[11]KwaZulu-Natal Research Innovation and Sequencing Platform (KRISP), Nelson R Mandela School of Medicine, University of KwaZulu-Natal, Durban 4001, South Africa.

* Corresponding Author: houriiyah@sun.ac.za

Summary

Oropouche virus (OROV) is an emerging arbovirus with increasing outbreaks in South America, yet its environmental drivers and potential range remain poorly understood. Using ecological niche modeling (ENM) with random forests, we assessed the environmental suitability of OROV and its primary vector, *Culicoides paraensis*, across Brazil and the Americas. We evaluated five pseudo-absence sampling techniques, considering pseudo-absence ratios, buffer radii, and density smoothing factors to determine the most effective modeling approach. Key environmental predictors included humidity, agricultural land-use, and forest cover, while temperature had minimal influence for both the virus and the vector. The resulting suitability model identifies high transmission risk areas in Central and South America, and reveals that environmental suitability patterns align with seasonal fluctuations in case numbers, with peaks in Amazonian states at the beginning of the year and an expansion into non-Amazonian regions later in the year. A bivariate suitability map highlighted strong spatial overlap between OROV and *Culicoides paraensis*, with potential co-suitability areas with *Culex quinquefasciatus* mosquito, a suspected secondary vector. These findings enhance understanding of OROV transmission dynamics, supporting risk assessment, surveillance, and vector control strategies.

Keywords: Arboviruses, Oropouche virus, *Culicoides paraensis*, Environmental niche models, Pseudo-absence sampling

1. Introduction

Oropouche virus (OROV) is an emerging arthropod-borne virus responsible for frequent and widespread outbreaks in South America, particularly in Brazil over the last few years. Since its discovery in 1955, OROV has caused numerous epidemics, with over half a million reported cases across several South and Central American countries, including Brazil, Cuba, Peru, Colombia, and Panama [1,2]. The virus is primarily transmitted by *Culicoides paraensis*, a biting midge that can occur all year round in urban and peri-urban areas[3] although other potential vectors have been implicated in its transmission cycle such as *Culex quinquefasciatus*[4–7]. The symptoms of Oropouche fever, including high fever, headache, and joint pain, are often misdiagnosed as dengue or other febrile illnesses, contributing to underreporting and gaps in surveillance [8]. While historically confined to the Amazon Basin and northern Brazil, OROV is increasingly being detected in new geographic regions, raising concerns about its potential expansion[9–11].

The 2023–2024 OROV outbreak in Brazil has been particularly alarming, with a rapid rise in cases across multiple states and 14,613 reported cases up till early 2025[12]. This surge has been attributed to changing land-use patterns, urbanization, and shifting climate conditions that may alter the ecological niche of both the virus and its vectors[9,11,13]. In 2024, reemergence and rapid epidemic expansion of OROV in Brazil and neighbouring countries[14], including, for the first time, transmission beyond the Amazon basin[9,10], and fatal cases[15]. In a previous study, we investigated the link between environmental covariates and OROV transmission in Brazil prior to and following amplified transmission, and pointed to a potential shift in the ecological niche of the virus preceding the epidemic[11]. This underscores a critical need for a comprehensive continental-scale assessment of OROV transmission potential and its vector. Developing detailed suitability maps can provide valuable insights into areas at risk, guiding public health interventions. Incorporating key environmental factors such as climate, land use, and vector ecology will improve our understanding of the conditions that facilitate virus persistence and spread.

Ecological niche modeling (ENM) is widely used in species ecology to predict species distributions (plants and animals) based on environmental conditions. More recently, it has been applied in disease ecology, particularly for vector-borne diseases, to assess transmission risk and identify high-risk areas for outbreaks[16,17]. While ENMs are widely used to predict vector environmental suitability based on presence-only data and environmental variables, their application to enumerate populations at risk of disease has also proved useful, improving surveillance and control strategies[18]. Various ENM approaches exist, including statistical models (e.g., Generalized Linear Models, Generalized Additive Models), envelope models (e.g., Maximum Entropy, Surface Range Envelope), and machine learning

algorithms (e.g., Random Forest, Boosted Regression Trees, Artificial Neural Networks). These models often rely on pseudo-absence data when true absence data is unavailable, using these points to contrast presence locations. While random sampling is commonly used to generate pseudo-absence data[19,20], more informed approaches have been suggested that enhance ecological relevance and potentially improve model accuracy. Informed sampling techniques incorporates spatial or environmental constraints, such as buffer zones around presence points (geographic-weighted exclusion)[21] or unsuitable environmental conditions (environmental-weighted exclusion)[19,22]. However, the impact of these methods on the resulting model outcomes has not been assessed for OROV.

In this study, we use random forest (RF) modeling to investigate the environmental suitability of OROV and its primary vector, *C. paraensis*. We evaluate the impact of five pseudo-absence sampling techniques to determine the most effective approach for modeling OROV distribution. We generate monthly environmental suitability predictions for OROV across Brazil and spatial continental-scale predictions across the Americas based on the consensus suitability model, which integrates predictions from multiple pseudo-absence sampling techniques. This approach ensures that both seasonal transmission patterns and broader geographic risk areas are captured with improved reliability. Additionally, we examine key environmental predictors influencing OROV transmission and assess the spatial overlap between the virus and its vectors. Finally, we construct bivariate suitability maps to explore potential co-occurrence zones between OROV, *C. paraensis* and *Cx. quinquefasciatus*, the suspected secondary vector. By identifying high-risk areas and key environmental drivers, this study provides critical insights into OROV transmission dynamics, to better inform surveillance and vector control strategies.

2. Results

Performance Across Pseudo-Absence Sampling Strategies

We tested five pseudo-absence sampling strategies under different pseudo-absence ratios: (1) Random sampling, where pseudo-absences were randomly selected across the study area, assuming a uniform probability of species absence; (2) Geographic sampling, which constrained pseudo-absences within a defined radius around presence points (See illustration in **Supplementary S3B)**; (3) Density-weighted geographic sampling, which incorporated the density of presence points into pseudo-absence selection, ensuring absences were more likely to be placed in areas with higher sampling effort, where the virus was likely searched for but not detected; (4) Density-weighted population-based sampling,

which further refined selection by integrating both the density of occurrence points and human population density, emphasizing areas of higher human interaction; and (5) Target group-based sampling, which used the distribution of other arboviruses (dengue, chikungunya, yellow fever, and Zika) to guide pseudo-absence selection, assuming that OROV surveillance would follow a similar spatial pattern.

The performance of ENMs varied across different pseudo-absence (PA) sampling strategies, with notable differences observed across PA ratios, buffer radii, and KDE smoothing factors. To evaluate model performance, we used the Boyce Index (BI), a presence-only metric that assesses how well predicted suitability aligns with independent occurrence data. A higher BI value indicates stronger agreement between the model's predictions and observed presence locations, making it particularly useful for evaluating models that rely on pseudo-absence data. Among the five sampling techniques assessed, the target group-based Sampling approach yielded the highest BI of 0.96 (ROC = 0.9) under a PA ratio of 1:1, a buffer radius of 50-500 km and a KDE smoothing factor of 5 (**Figure 1A**). In contrast, random sampling consistently produced the lowest BI values, with a maximum of 0.72 at a PA ratio of 10,000 (ROC = 0.509). Model performance was generally better across the different sampling techniques when a PA ratio of 1:1 was applied (See **Supplementary Figure S1**). However, we see less variability in model performance for a balanced presence-absence ratio (1:1, n=400) and for a high pseudo absence numbers (n=10,000) (See **Supplementary Figure S1**). When examining the effect of buffer radii, we observe less variability in model performances when a more restrictive geographic buffer is applied, in this case between 50 - 150 km and 50 - 300 km (see **Supplementary Figure S1**). Overall, smaller KDE smoothing factors were associated with improved model performance across sampling techniques, PA ratios, and buffer radii, suggesting that less smoothing enhances the model's ability to capture finer-scale patterns.

The spatial predictions of environmental suitability also varied across sampling strategies (**Figure 1B**). Across all methods, regions of highest suitability (red areas) were predominantly concentrated in areas where known virus occurrences have been reported, particularly in the northern and coastal regions of Brazil, including parts of the Amazon Basin. However, the extent and specificity of these high-suitability areas varied depending on the PA sampling technique applied. The best-performing model for geographic sampling produced a more spatially constrained suitability pattern (**Figure 1B**), with high suitability concentrated in regions with reported occurrences, while other areas exhibited very low suitability values. This pattern may be attributed to the restricted buffer of 50–150 km, which likely limited the spatial extent of pseudo-absence selection, resulting in a more localized prediction of environmental suitability. The density-weighted population-based sampling approach generated a broader environmental suitability distribution across the country, while exhibiting a more spatially constrained high-suitability pattern along densely populated coastal regions. This outcome is

likely a result of the underlying methodology, in which pseudo-absences were predominantly sampled near populated areas, thereby refining suitability predictions in urbanized regions while maintaining a wider overall suitability range. The target group-based sampling method generated the most spatially precise predictions, with high-suitability areas concentrated along humid, densely forested, and agriculturally active zones.

The variable importance analysis revealed that humidity was the most influential predictor, contributing 16.0% to the model's explanatory power (**Figure 1C**). Other key predictors included banana harvested area (6.4%), elevation (6.4%), and forest cover (3.6%), highlighting the role of land-use and topographic features in shaping environmental suitability for virus transmission. In contrast, temperature variables contributed only 0.4%. The moderate contribution of agricultural land-use variables (e.g., sugarcane, cocoa, and cassava harvested areas) suggests that human-modified landscapes may influence transmission dynamics.

Figure 1. Comparison of sampling techniques, variable importance, and spatial suitability predictions. (A) Boyce Index (BI) performance across five pseudo-absence sampling techniques (Random Sampling, Geographic Sampling, Density-Weighted Geographic Sampling, Density-Weighted Population-Based Sampling, and Target

Group-Based Sampling) with varying PA ratios and buffer radii. Higher BI values indicate better model performance. (B) Spatial distribution of habitat suitability predicted under each sampling strategy (predictions from the best performing model under each technique), with darker red areas indicating higher suitability. The BI for each method is displayed in parentheses. (C) Variable importance analysis, showing the relative contribution of explanatory variables to the species distribution model (evaluated under Target Group-Based Sampling model). The dark red vertical line (0.01) represents the mean relative importance across variables (and models pseudo absence runs).

Spatiotemporal Consensus Suitability Maps across Brazil

To obtain an overall OROV disease risk map for Brazil, we calculated a consensus map by integrating predictions from the best-performing models under each pseudo-absence sampling technique. We assigned ranks based on the BI score, converted them into weights by dividing each model's rank by the sum of all ranks, and used these weights to generate a final weighted environmental suitability map, referred to as the consensus map. The consensus map of environmental suitability (**Figure 2A**) reveals spatial heterogeneity in OROV transmission potential across Brazil, with highly suitable regions concentrated in the Amazon Basin and along major river systems. The highest suitability is observed in northern and central regions, particularly in the states of Amazonas (AM), Pará (PA), Rondônia (RO), and Maranhão (MA). Notably, coastal regions of northeastern and southeastern Brazil also exhibit high suitability, suggesting that environmental conditions outside the traditional endemic zone may support virus circulation. Areas with low suitability are primarily located in the central-west and southern regions, where climatic and ecological conditions may be less conducive to sustained transmission.

The suitability index was then projected over a monthly time interval in Brazil, considering variations in climatic variables. This temporal analysis (**Figure 2C**) highlights seasonal patterns in environmental suitability which closely align with reported case counts in the country. The suitability index is highest between January and May (>0.5) particularly in the Amazonian states, coinciding with the period of peak case numbers in Amazonian states. The decline in environmental suitability from June to September closely coincides with the drop in reported case numbers, suggesting that seasonal changes during this period create less favorable conditions for virus transmission. Towards the end of the year, environmental suitability begins to increase once again, coinciding with a rise in reported cases, particularly in non-Amazonian states. The monthly suitability maps (**Figure 2B**) further illustrate the dynamic seasonal shifts in transmission potential coinciding with increases and decrease of reported cases.

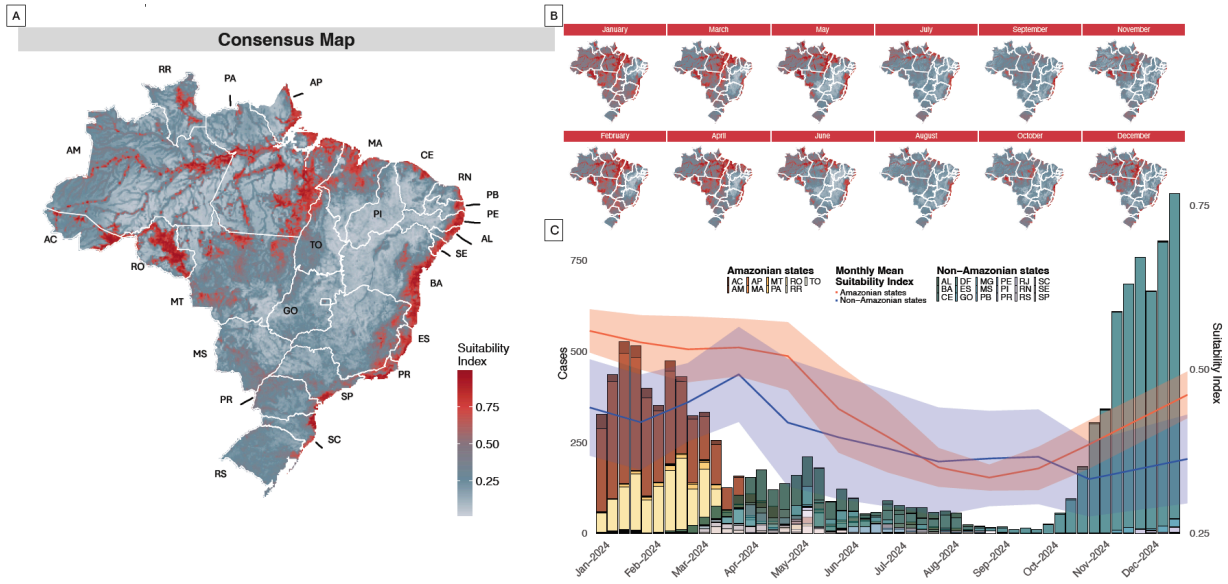

Figure 2 Consensus map and temporal environmental suitability trends. (A) The consensus map of environmental suitability for Oropouche virus transmission across Brazil, highlighting areas with persistent high suitability (red) and regions with lower suitability (blue). (B) Monthly projection of environmental suitability index across Brazil (maps) with temporal trends in case counts (stacked bars) and suitability index (lines) for the year 2024, with separate trends for Amazonian and non-Amazonian states. Shaded regions represent the variability in suitability estimates, with darker lines indicating mean suitability.

Continental Predictions of OROV and its primary vector, *C. paraensis,* across the Americas

The spatial predictions of OROV environmental suitability across the Americas reveal distinct high-risk regions concentrated in tropical and subtropical areas of South and Central America (**Figure 3A**). The model identifies high suitability along the Amazon Basin, the Atlantic Forest of Brazil, and portions of Colombia and Peru, reflecting known virus circulation areas. In Central America, suitability is notably high in Panama, Costa Rica, and parts of Honduras and Nicaragua, suggesting potential transmission risk beyond traditionally recognized endemic zones. Some coastal areas of Mexico and the Caribbean also exhibit moderate suitability, though these predictions are less pronounced **(Figure 3A)**. The United States of America exhibits moderate to low environmental suitability for OROV transmission, with only small, isolated areas of moderate suitability along the southeastern coastline and parts of the Gulf Coast.

The uncertainty map (**Figure 3B**) provides insight into the stability and consistency of model predictions across different pseudo-absence sampling strategies. The uncertainty values are derived as the variation across the five best-performing models used to build the consensus map. This variation quantifies the differences in predictions among these top models, highlighting areas where model agreement is high or low. Lower uncertainty (green areas) is observed in well-documented endemic

regions, particularly in northern Brazil and part of the Amazon Basin, where high suitability predictions remain stable across all models. Conversely, higher uncertainty (orange to yellow regions) is present in parts of Central America, southern Brazil, and parts of the Andes, suggesting that predictions in these areas are more sensitive to the choice of pseudo-absence sampling technique.

We also built an ENM for the primary vector, *C. paraensis*, using the best-performing pseudo-absence sampling technique identified in the virus model evaluation. The variable importance analysis from the vector model (**Figure 3C**) highlights banana harvested area (11.6%) as the strongest predictor of the vector's environmental suitability. Other important predictors include sugarcane harvested area (4.8%), cropland natural vegetation (2.8%), soil moisture (1.2%) and humidity (1.2%), reinforcing the role of agricultural landscapes and moisture availability in shaping the vectors' environmental niche. Notably, temperature variables ($\leq 0.4\%$) contributed minimally to the model.

The vector's suitability map (**Figure 3D**) mirrors a similar geographic pattern as the virus, particularly in Brazil, the Amazon Basin and parts of Central America. High suitability for the vector is observed in Central America, countries such as Costa Rica (CRI) and Panama (PAN) particularly in lowland and humid forested areas, aligning with the ecological preferences of *C. paraensis*. We also observe high environmental suitability areas concentrated in moist areas of Colombia and parts of the United states, particularly Florida.

Exploring the overlap of viral-vector predictions and the possibility of suspected secondary vector, *Culex quinquefasciatus*

Given the similarities in spatial patterns, examining the bivariate suitability map of the viral and vector suitabilities together can provide insight into where both OROV and its vectors are likely to co-exist and sustain transmission. Given its widespread distribution, ecological adaptability, and documented detection of OROV RNA in field-caught specimens, *Cx. quinquefasciatus* has been proposed as a potential secondary vector, warranting further investigation into its role in OROV transmission [4]. We constructed two bivariate maps: one depicting the relationship between OROV and its primary vector (*C. paraensis,* **Figure 4A**) and another between OROV and its secondary vector (*Cx. quinquefasciatus*, **Figure 4B**), using the suitability map from Alaniz et al. (2019) [23]. The bivariate maps reveal that regions with high suitability for both the virus and primary vector (*C. paraensis*) are concentrated in northern South America, Central America, and coastal Brazil, reinforcing the role of this vector in OROV transmission. We can observe the broader distribution of *Cx. quinquefasciatus* which extends further south into Argentina, Chile, and Uruguay, suggesting that transmission risk may not be limited to tropical areas. In the Caribbean, notably, *Cx. quinquefasciatus* appears slightly more suitable in Cuba than *C. paraensis* (**Figure 4B-inset**). Correlation analysis indicates a strong association between the virus and its primary vector ($r = 0.72$), while the correlation between OROV

and *Cx. quinquefasciatus* is notably weaker (r = 0.23). While *C. paraensis* remains the dominant driver of OROV transmission, the presence of *Cx. quinquefasciatus* in more temperate regions suggests potential areas of co-suitability where further investigation is needed.

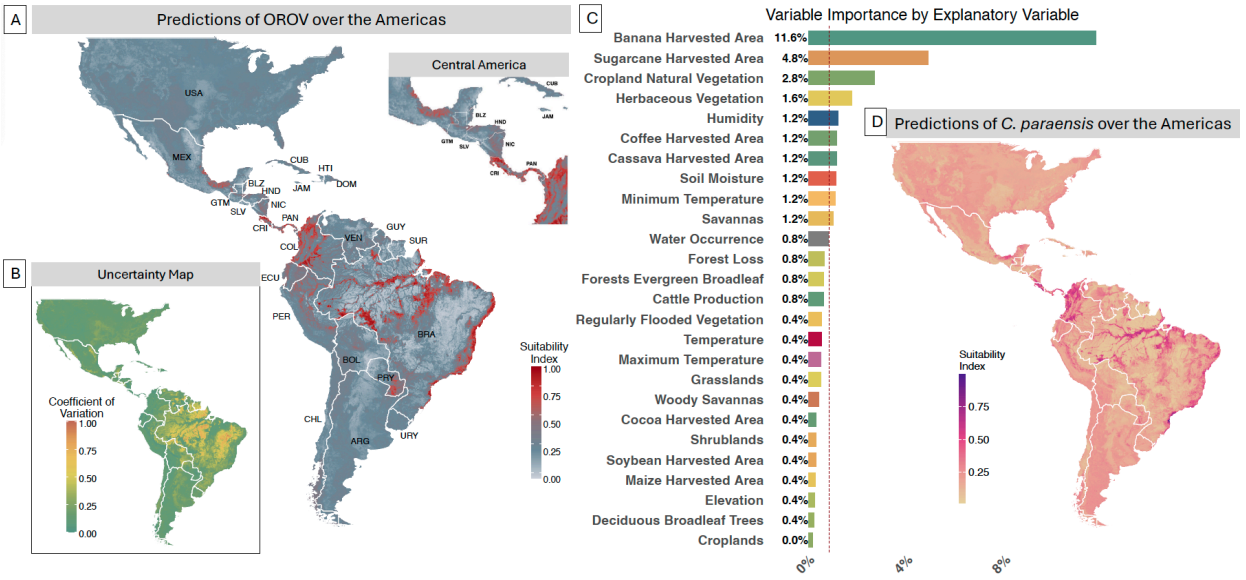

Figure 3 Predicted Environmental Suitability for Oropouche Virus (OROV) and its primary Vector, *Culicoides paraensis*, across the Americas. (A) Predicted environmental suitability for Oropouche virus transmission across the Americas. The inset highlights suitability predictions for Central America, including Panama (PAN), Costa Rica (CRI), Nicaragua (NIC), Honduras (HND), El Salvador (SLV), Guatemala (GTM), Belize (BLZ), Cuba (CUB) and Jamaica (JAM). (B) Uncertainty map displaying the coefficient of variation, across models built under different pseudo-absence sampling techniques. (C) Variable importance analysis for the vector, *C. paraensis*, ranking the contribution of explanatory variables to model predictions. On the right, environmental suitability predictions for *C. paraensis* across the Americas. The dark red vertical line represents the mean relative importance across variables (and models pseudo absence runs). (D) Predicted environmental suitability for *C. paraensis* distribution across the Americas.

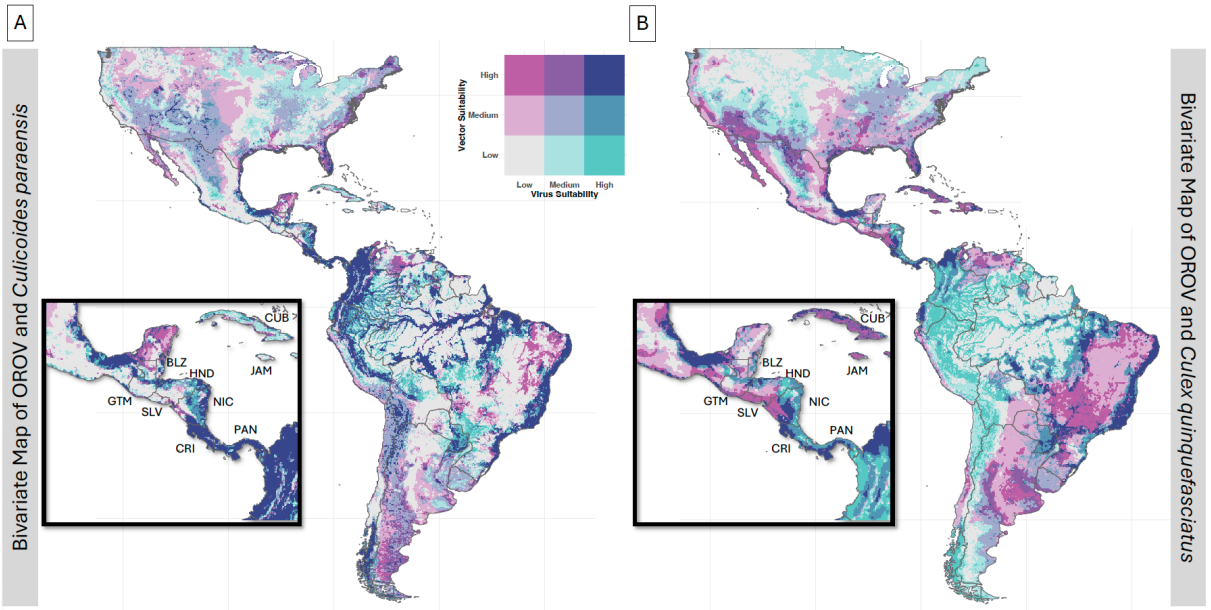

Figure 4 Bivariate suitability maps of Oropouche virus (OROV) and its vectors: (A) *Culicoides paraensis* (primary vector) and (B) *Culex quinquefasciatus* (suspected secondary vector; data obtained from [23]). The color gradient represents the combined suitability of OROV and each vector, with light gray indicating low suitability for both, pink/purple hues representing higher suitability for the vector, blue tones indicating higher suitability for the virus, and dark purple signifying high suitability for both. Insets highlight Central America and the Caribbean.

3. Discussion

Here, we present some of the first uses of ecological niche models application in OROV disease ecology and virus transmission. Unlike plants and animals, viruses depend on vector-host interactions, human movement and environmental persistence, making their spatial dynamics more complex[24,25]. Given these differences, we assessed whether traditional species modelling frameworks effectively capture virus distributions, focusing on the role of pseudo-absence selection and environmental drivers. Additionally, we investigated the environmental suitability of OROV alongside its primary vector, *C. paraensis*, and the potential role of *Cx. quinquefasciatus* as a secondary vector. In summary, we obtain a comprehensive continental assessment of the risks of transmission of this virus, which will be critical for public health planning.

In this study, for the OROV models, the target group-based sampling technique for pseudo-absences outperformed random sampling, particularly under small PA ratio[26]. The target group-based sampling technique produced the highest Boyce Index (BI = 0.96, ROC=0.904) with a small PA ratio and and the most spatially refined suitability predictions, supporting the idea that pseudo-absence selection strategies based on known virus occurrence records improve model accuracy[19]. Milanesi et al.[27]

reported that an observer-oriented approach using occurrences of a target group species as pseudo-absences improved ENM predictive accuracy compared to random pseudo-absences. Random sampling in our case resulted in relatively poor model accuracy across small PA ratios, which is a well-documented limitation in species distribution models when absences are not ecologically meaningful[28]. The strong performance of density-weighted sampling approaches suggests that incorporating demographic data into pseudo-absence selection improves the model's ability to capture virus transmission patterns. While target group background sampling shows promise in addressing sampling bias and improving SDM performance, results may vary depending on the specific implementation and ecological context. Careful consideration should be given to defining appropriate target groups and the sampling domain, environmental heterogeneity, and resulting spatial predictions which is crucial for developing biologically realistic and fit-for-purpose habitat models [27,29].

The strong performance of both 1:1 PA ratios and 10,000 pseudo-absences suggests that model accuracy benefits from either balanced contrast or extensive background coverage. A balanced contrast (1:1 PA ratio) means that presence and pseudo-absence points are equally weighted, preventing biases that may arise when one class dominates the dataset. Extensive background coverage (10,000 pseudo-absences) allows the model to sample a wide range of environmental conditions, improving generalization by better representing areas where the virus is unlikely to occur[19,30]. In contrast, intermediate PA ratios (1:5, 1:10 with 2,000 – 4,000 pseudo-absences) do not provide enough contrast as 1:1 nor enough environmental representation as 10,000, leading to weaker model performance. While some PA ratios performed well under specific pseudo-absence sampling techniques, no single ratio consistently outperformed others across all approaches. This suggests that the most effective pseudo-absence ratio depends on the chosen sampling technique and the ecological or spatial characteristics of the target species or pathogen.

The variable importance analysis (**Figure 1C & Figure 3C**) revealed notable similarities in the environmental drivers of OROV and *C. paraensis* suitability. Humidity emerged as the strongest predictor for OROV (16.0%), likely due to its role in vector survival, as it also influenced *C. paraensis* presence (1.2%). Land-use variables, particularly banana harvested area, were key predictors for both the virus and vector, possibly due to *C. paraensis*' preference for breeding in decaying vegetation and agricultural waste[7,11,13]. Previous studies have reported that *C. paraensis* utilizes crop residues, such as banana and cocoa remains, as breeding sites in man-modified landscapes[7]. Our study found soil moisture to significantly influence the vector's distribution (**Figure 3C**), which aligns with the vector's lifecycle stages, including egg-laying, larval development, and adult survival[31]. As such, it serves as a hotspot for vector populations. Moreover the larvae of *C. paraensis* not only prefers moisture but also thrive in microhabitats such as tree holes, decaying organic matter whereby they are particularly drawn to rotting banana and plantain stalks[32], which we

also observed in this study (**Figure 3C**). Temperature had minimal influence on OROV suitability (≤ 0.4%) and only slightly higher for *C. paraensis*, unlike many mosquito-borne viruses, where temperature is key to vector competence and viral replication[33]. This suggests that factors like vector behavior, host movement, and environmental persistence play a greater role in OROV transmission. Thus, modeling the virus separately from its vector is crucial, as relying solely on vector presence could overestimate risk areas.

The spatial and temporal dynamics of OROV suitability revealed in this study highlight the seasonal and geographic variability in transmission risk across Brazil. The consensus map (**Figure 2A**) indicates that high suitability is not limited to the Amazon Basin but extends along major river systems and into coastal regions of northeastern and southeastern Brazil, suggesting that environmental conditions outside traditionally recognized endemic zones may support virus circulation. This aligns with recent studies showing that vector-borne disease distributions are influenced by land-use change, deforestation, and urbanization, which can create new ecological niches for disease transmission[3].

The seasonal fluctuation in suitability (**Figure 2B**) underscores the importance of climatic drivers in modulating OROV transmission potential. We found that the highest suitability and case numbers coincide with the rainy season (January–May 2024 in the Amazonian region) which aligns with previous studies that have observed Oropouche outbreaks occurring during the rainy season[2,8,13], followed by a decline during the drier months (June–September), which likely results from reduced vector populations and lower environmental favorability for transmission (Feitoza et al., 2023). However, the resurgence of suitability towards the end of 2024, particularly in non-Amazonian states, suggests that seasonal transmission risk extends beyond traditionally endemic regions. This pattern may be driven by vector population dynamics, human movement, and changing land-use patterns, emphasizing the need for continuous surveillance beyond peak transmission months. The expansion of high suitability into southern and southeastern states by November–December 2024 highlights potential emerging hotspots, reinforcing the necessity of adaptive public health interventions that account for shifting transmission risks across both time and space.

The spatial predictions for OROV suitability indicate a strong alignment with known virus circulation areas, particularly across the Amazon Basin, Atlantic Forest, and portions of Central America (**Figure 3A**). However, the extension of high suitability into regions where OROV has not been extensively documented, such as southern Brazil and areas of the Andes in South America, suggests potential underreporting or conditions favorable for future virus expansion. Our virus suitability map also revealed a more widespread distribution in northern South America and parts of Central America exhibit high suitability for OROV. In Central America, coastal regions of Nicaragua, as well as parts

of Costa Rica and Panama, exhibit high suitability for the virus. This observation also aligns with the suspicion that regions in Central America have a high number of unreported cases[2]. However, our principal component analysis (PCA) comparison between the modeling area and the prediction area (see **Supplementary Figure S2**) indicates that some environmental conditions in the prediction area extend beyond the range of the training data.

In contrast, *C. paraensis,* revealed a slightly more conservative distribution, with high suitability in Brazil, Columbia, Central America and coastal region of Mexico and Florida in the United States. This geographic distribution pattern of *C. paraensis* aligns with its preference for humid environments and its ability to thrive in urban areas[2,3]. The relationship between OROV and its vector is key to understanding transmission dynamics. While vector presence, environmental conditions, and human activity shape transmission risk (Ferraguti et al., 2021; Zouache et al., 2014), the geographic overlap between virus and vector suitability is not absolute. Areas with high OROV suitability but lower predicted vector presence suggest the potential involvement of a secondary vector, warranting further investigation into both the primary vector's ecology and the possibility of alternative transmission routes.

Despite *C. paraensis* being recognized as the primary vector of OROV, the limited research on vector competence leaves gaps in our understanding of its full transmission cycle. A systematic review found that, in the six decades between OROV's discovery and the 2023–24 outbreak, only seven vector competence studies had been published (Gallichotte et al., 2024). The recent OROV outbreak in Cuba, which coincided with a larger epidemic across the Americas, further raises questions about vector competence and transmission dynamics. Notably, Benitez et al. (2024) detected OROV RNA in *Cx. quinquefasciatus* mosquitoes, providing potential evidence of a secondary vector contributing to transmission. Our bivariate map also revealed that Cuba was at higher risk of OROV transmission with *Cx. quinquefasciatus* as a vector than *C. paraensis* (**Figure 4**). Given that virus distribution is shaped by both ecological and anthropogenic factors (Brunker et al., 2018; Finlay & Luck, 2011), further research is needed to assess the role of alternative vectors and environmental conditions that may facilitate virus persistence beyond its primary transmission pathways. Understanding how multiple vectors interact with OROV across different ecological settings is essential for refining targeted surveillance and control strategies (Ferraguti et al., 2021; Zouache et al., 2014), particularly in regions where virus and vector suitability do not fully align.

A potential limitation of this study is that our PCA comparing the modeling and prediction areas (refer to **Supplementary Figure S2**) reveals that certain environmental conditions in the prediction area fall outside the scope of the training data. This emphasizes zones with unique environmental characteristics and stresses the need for careful interpretation in these areas, as extrapolation may lead

to increased uncertainty. Moreover, we make no differentiation between OROV lineages. In particular, the circulation of novel reassortant strains across South America could indicate differential adaptation to ecological niches based on viral genetic diversity[11,34]. Variants circulating in sylvatic versus urban environments may exhibit distinct environmental tolerances and transmission dynamics. This heterogeneity could significantly influence the virus's spatial distribution. Additionally, little is known about the ecology of the primary vector, *C. paraensis*, with few studies investigating its geographic range, habitat preferences, or physiological constraints. Mechanistic laboratory experiments assessing vector competence, survival limits, and environmental tolerances remain scarce, limiting our ability to refine vector distribution models and fully understand its role in OROV transmission.

In conclusion, this study underscores the intricate relationship between environmental and climatic factors in shaping the distribution of OROV and its primary vector, *C. paraensis*. While evaluating different pseudo-absence sampling techniques and identifying key environmental predictors, we projected the spatial distribution of both the virus and vector across the Americas, identifying regions with high transmission potential and potential range expansions driven by climate and land-use changes. Additionally, we conducted monthly environmental suitability projections across Brazil, capturing seasonal fluctuations in OROV transmission risk, and we raise concerns about the possibility of transmission via secondary vectors. These findings provide valuable insights for refining predictive models and improving targeted surveillance and control strategies. A comprehensive understanding of these dynamics is essential for anticipating future OROV outbreaks and mitigating their impact on public health.

4. Methodology

4.1 Ecological Niche Modelling of Oropouche Virus

Ecological niche modelling (ENM) is a powerful approach for predicting the potential distribution of species and pathogens by identifying relationships between occurrence data and environmental variables[35]. Model selection generally depends on the type and quality of data available[36]. In this study, we apply ENM to assess the distribution of OROV using random forests (RF), a widely used machine learning technique known for its robustness in handling complex, high-dimensional ecological data[37]. RFs build a large ensemble of decision trees using random subsets of the training data, where each decision split is determined by a randomly selected subset of predictor variables[37–40]. The process starts by creating multiple bootstrapped samples, each containing the same number of

data points, selected with replacement. Each sample is then used to train a classification tree, with splits based on the best predictor among a randomly chosen subset of candidate variables. Once the trees are fully trained (with a maximum of 500 trees), they are used to predict the 'out-of-bag' (OOB) samples - data points that were not included in the bootstrapped sample. These OOB samples are crucial for estimating the model's accuracy and errors, and the misclassification rate of each tree is computed using OOB samples[38,41].

ENMs typically rely on "background" or "pseudo-absence" data when true absence data is unavailable, using these as a contrast to presence locations in the model. A critical challenge in building the appropriate ENM is the selection of appropriate pseudo-absence data. To address this, we evaluate multiple pseudo-absence sampling strategies within the RF framework to determine the most suitable approach for modelling OROV's environmental suitability distribution. The RF models are implemented using the R package biomod2 (version 4.2-5-2), allowing for a comprehensive assessment of how different pseudo-absence selection methods influence model performance. The code used for the analyses in this study can be found at [repository link].

4.1.1 Virus Occurrence Data

Disease presence points of Oropouche were obtained and compiled from various locations in Brazil (molecular testing and sequencing records) from the years 1957 to 2024. Epidemiological data on OROV cases were retrieved from the Brazilian Ministry of Health, accessible at https://www.gov.br/saude/pt-br/assuntos/saude-de-a-a-z/o/oropouche. The data set includes confirmed case reports from all Brazilian states where OROV cases have been notified, including but not limited to Acre (AC), Alagoas (AL), Amazonas (AM), Bahia (BA), Ceará (CE), Minas Gerais (MG), Pará (PA), Rio de Janeiro (RJ), and São Paulo (SP). The data cover the years 2023 and 2024, organised by epidemiological week of reporting, and include key variables such as the municipality, state, and the year of occurrence. This data was geocoded at the municipality level and occurrence data were deduplicated by month. Additional OROV occurrence data was gathered and geocoded from all records in the GBIF (years: 1957-present) and Genbank (years: 2015-present) databases. After deduplicating all occurrence records, a total of 450 unique sampling location points remained (**Supplementary Figure S3A)**, covering the years 1957 to 2024, with the majority (~85%) sampled in 2023-2024. For model development, the dataset was split into training and testing subsets, with 400 presence points used for training and randomly selected 50 presence points kept for model evaluation.

4.1.2 Pseudo-absence sampling method

RF models require both presence and absence data to estimate the relationships between environmental predictors and species occurrence. However, true absence data are rarely available in ecological studies, particularly for infectious diseases and their vectors, due to the challenge of confirming species or pathogen absence at any given location. In the absence of true absence data, pseudo-absence points are generated and used in modelling. In this study, we compared the performance of five absence generation approaches:

1. **Random Sampling:** This method involves generating pseudo-absence points by randomly selecting locations within the study extent that did not overlap with presence points. This method assumes a uniform probability of species absence across the landscape, making it straightforward to implement.
2. **Geographic Sampling:** In this approach, pseudo-absences were generated within a defined geographic buffer or step-length around presence points. Unlike Random Sampling, this method first sets a spatial constraint around presence locations before randomly selecting pseudo-absence points within that area. By confining pseudo-absence points to areas near presence locations, the method accounts for the fact that species may be influenced by local environmental and spatial conditions, providing a more ecologically meaningful sampling strategy (See illustration in **Supplementary Figure S3-PanelB**) .
3. **Density-Weighted Geographic Sampling:** This method incorporates the density of occurrence points to guide pseudo-absence selection[42,43]. This method was tested both with and without the use of geographic buffers around presence points. By using the density of presence points as a proxy for sampling effort, pseudo-absences were more likely to be generated in areas with a higher concentration of presence observations. This reflects the reality that sampling is often biased toward accessible or frequently visited locations, the aim is to ensure that pseudo-absence points align with regions where sampling is likely to have occurred but the virus was not detected.
4. **Density-Weighted Population-Based Sampling:** Building upon the density-weighted geographic sampling approach, this method further refines pseudo-absence selection by integrating both the density of occurrence points and human population density. It was tested both with and without the use of geographic buffers around presence points, allowing for flexibility in accounting for spatial constraints. By incorporating population density, this approach reflects the critical relationship between human activity and the virus' occurrence, particularly for species like OROV that depend on human hosts for transmission. The aim of this approach is to emphasise areas with higher human interaction where the species is absent but sampling efforts are likely.

5. **Target Group-Based Sampling:** Similarly, this approach, derived from Phillips et al.[44], uses all occurrences of a predefined species group (the target group), in this case, other arboviruses such as dengue, chikungunya, yellow fever, and Zika[45]. The method uses the sampling density of these other arboviruses to guide the selection of pseudo-absence points, with the assumption that the sampling effort for the species of interest (OROV in this case) would follow a similar strategy. This approach was applied both with and without geographic buffers around presence points.

We evaluated those five pseudo-absence sampling strategies across five pseudo-absence ratios (PA ratio), four geographic buffer radii, and three Kernel Density Estimation (KDE) smoothing factors, leading to a systematic assessment of pseudo-absence selection effects

For each sampling strategy, we sampled pseudo-absences in the ratio of 1:1, 1:2, 1:5, 1:10 with respect to the presence points and a fixed number of 10,000 presence points across Brazil. For clarity, we will hereafter refer to this as the PA ratio. To account for spatial constraints in pseudo-absence selection, we investigated geographic buffers of 50–150 km, 50–300 km, and 50–500 km around presence points. A minimum buffer of 50 km was applied to ensure that pseudo-absence points were not placed in the exact same pixel as presence points.

For density weighted approaches, to quantify the spatial distribution of presence points, we applied Kernel Density Estimation (KDE) with a Gaussian kernel to generate a continuous density surface. The degree of smoothing is controlled by the bandwidth parameter (σ), which defines the spatial scale over which density is estimated. Given our Cartesian coordinate system, σ is expressed in degrees, where 1 degree $\approx$ 111 km. We evaluated three bandwidths (σ = 1, 3, and 5) to assess the impact of kernel smoothing. Regions with higher density indicate areas of greater sampling effort, guiding pseudo-absence selection to align with areas that were likely sampled but where the virus was not detected (See illustration in **Supplementary Figure S3C**).

The combinations of sampling strategies, PA ratios, buffer radii, and KDE smoothing factors resulted in 200 models (see **Supplementary Figure S4**). Each model was replicated three times with replacement to assess variability in pseudo-absence selection.

4.1.3 Environmental Variables

In this study, we considered a total of 29 environmental variables, including climate-based and land-use variables. These environmental variables were chosen based on their known influence on vector habitat suitability and viral transmission dynamics[2,3,46]. After removing highly correlated variables ($r > 0.8$), except for maximum and minimum temperature to assess an optimum temperature effect, we retained 26 variables. All variables were in raster format, with all raster maps standardized to the lowest available resolution (~27 km²) to ensure consistency across datasets. For climate variables, presence points were matched to their corresponding climate data based on the month of collection, ensuring temporal alignment between observed occurrences and environmental conditions at the time of sampling. The environmental variables were also acquired for the Americas (excluding Alaska and Canada) for projections outside of Brazil. Environmental variables for this study were sourced from publicly available remote sensing datasets and detailed information can be found in **Supplementary Table S1**.

4.2 Model Evaluation

To be able to compare the predictive performance of the ENMs built under different sampling techniques, we used the BI[47,48]. The BI quantifies how well the predicted suitability values align with the actual occurrence points in the independent test dataset, making it particularly suitable for presence-only data. The BI is computed by comparing the frequency of predicted suitability values at observed presence locations (testing dataset) against the frequency of suitability values at randomly selected background points.

The index evaluates the relationship between habitat suitability predictions and observed presence points by comparing the predicted frequency of presence points (Pi) to the expected frequency under random distribution (Ei) across suitability bins (i). The predicted-to-expected ratio ($Fi = Pi / Ei$) is then computed for each bin. To reduce sensitivity to bin selection, the BI was computed using a moving window approach[48,49]. This method smooths the P/E curve by shifting a window across the suitability range, reducing biases from arbitrary binning. The Spearman correlation coefficient is calculated between these ratios and the midpoints of the bins, producing the BI. The index ranges from -1 to 1, with 0 indicating that the model is not different from a chance model. This estimate, derived from fixed bins, is referred to as the original Boyce Index (OBI).

Additionally, model performance was internally evaluated across different pseudo-absence replicates within each sampling strategy. The Random Forest models were evaluated using a block cross-validation approach to address spatial autocorrelation[50]. The study area was divided into four

geographic blocks, designed to be of comparable size while also containing a minimum of 30 observations to maintain spatial independence between training and validation data. Models were trained on different combinations of these blocks and validated on the hold-out blocks. This method reduces the risk of overfitting and prevents performance inflation caused by spatial dependencies. We computed the True Skill Statistic (TSS) and the Receiver Operating Characteristic (ROC) curve for each model. These metrics were used to compare model performance and assess consistency across different sampling approaches. Full results, including TSS and ROC values, are provided in the Supplementary Materials (Annexe1).

4.2.1 Variable Importance

The contribution of each variable to species distribution prediction was determined by analysing the importance of each variable based on the best-performing model. We evaluated variable importance using a permutation-based approach implemented in the BIOMOD2 R package. For each variable, the procedure involves shuffling the original values of the variable and then generating model predictions using the shuffled data. The Pearson correlation coefficient (ϱ) between the original and shuffled predictions was computed, with variable importance defined as $1 - |\varrho|$, where a higher score indicates greater influence of the variable on the model. Specifically, a higher score reflects a lower correlation between the reference and shuffled predictions, suggesting that the variable plays a significant role in the model. This process is repeated five times for each variable, and the mean importance score is reported.

4.2.2 Monthly Projections and Predictions across the Americas

After generating models from the different pseudo-absence sampling techniques, we evaluated their performance using the BI and ranked them accordingly. The best-performing model from each sampling technique was selected and assigned a rank based on its BI score. Previous studies have demonstrated that ensemble modeling, which integrates predictions from multiple statistical and machine learning algorithms, improves model performance by accounting for variability across different modeling approaches[51,52]. In this study, we extend this concept by constructing a consensus environmental suitability map from the different pseudo-absence sampling techniques rather than different modeling algorithms.

To construct a consensus prediction, we calculated a weight for each model according to its rank. The model with the highest BI score received the highest rank (5), while the lowest-performing model received the lowest rank (1). We then converted these ranks into weights by dividing each model's rank value by the sum of all ranks, ensuring that higher-performing models contributed more to the

final prediction. These weights were then used to generate a final weighted environmental suitability map, integrating information from all sampling techniques, which, for simplicity, we refer to as the consensus map.

For monthly projections in Brazil, we produced suitability maps based on monthly 2024 climate variables, while keeping all other environmental predictors at their yearly values. This allowed us to capture seasonal transmission patterns influenced by climatic fluctuations. For temporal comparison with OROV recorded cases in Brazil, we computed the monthly mean environmental suitability index separately for Amazonian and non-Amazonian states to assess how suitability trends align with observed case fluctuations. For larger spatial-scale predictions, we applied the consensus model using mean annual climate variables to generate an overall environmental suitability map for the Americas (excluding Alaska and Canada). To assess the reliability of our spatial predictions, we performed a Principal Component Analysis (PCA) to compare the environmental niche of the modeling area with that of the prediction area. This allowed us to evaluate the extent of overlap and identify regions where predictions may extend beyond the range of sampled environmental conditions, providing insight into potential extrapolation uncertainty.

4.3 Primary vector and suspected secondary vector of Oropouche Virus

For the occurrence data of *C. paraensis*, the primary vector of OROV, we utilised geocoded records obtained from the Global Biodiversity Information Facility (GBIF, 2024) as well as data from several published studies[3,53–55]. After data cleaning, including duplicate removal and georeferencing verification, 78 occurrence points from Brazil were retained. However, this limited number of records may not fully capture the species' ecological range, making comprehensive modeling challenging.

We fitted a RF model using the target group-based approach for pseudo sampling based on the best performing model for OROV. Presence data from all species within the Ceratopogonidae family, to which *C. paraensis* belongs, were used to construct a sampling density map, assuming that the distribution of *C. paraensis* overlaps spatially with other closely related species. A total of 1,862 occurrence points for the Ceratopogonidae family were retrieved from GBIF (1945–2024), and after data cleaning, 286 uniquely geocoded records were retained.

To explore the potential overlap in environmental suitability between OROV and its vectors, we generated two bivariate suitability maps. This map visualized the co-suitability of OROV and *C.*

paraensis, as well as that of the suspected secondary vector, *Cx. quinquefasciatus*. A comprehensive suitability map for *Cx. quinquefasciatus* was obtained from Alaniz et al.[23], allowing us to assess potential regions where both primary and secondary vectors may facilitate OROV transmission.

Data Availability Statement

Current and future climate data are available at https://cds.climate.copernicus.eu/datasets. Anthropogenic data are available at https://www.earthdata.nasa.gov/. Data and code used in this study can be found at: https://github.com/CERI-KRISP/OROV_Vector_vs_Virus_Modelling

Declaration of interests

We declare no competing interests.

Contributors

J.P. and H.T. conceptualised and designed the study. J.P. analysed data, executed all primary data visualisations, and wrote the original draft. G.D. contributed towards the data extraction. M.G., L.A. and V.F. provided disease occurrence data. H.T., M.D., J.P., M.U.G.K, O.J.B. and A.L. contributed to methods development. C.B. and T.d.O. acquired funding for this study. H.T., M.D. and T.d.O supervised this work. All authors reviewed the manuscript.

Acknowledgements

CERI and KRISP are supported in part by grants from the Rockefeller Foundation (HTH 017), the National Institute of Health USA (U01 AI151698, also M.G.) for the United World Antiviral Research Network (UWARN), European Union's Horizon Europe Research and Innovation Programme (101046041), the Health Emergency Preparedness and Response Umbrella Program (HEPR Program), managed by the World Bank Group (TF0B8412), the Medical Research Foundation (MRF-RG-ICCH-2022-100069), the Wellcome Trust (228186/Z/23/Z), and the Novo Nordisk Foundation (NNF24OC0094346, also M.G. and

M.U.G.K.). O.J.B. was supported by a UK Medical Research Council Career Development Award (MR/V031112/1). M.U.G.K. acknowledges funding from The Rockefeller Foundation (PC-2022-POP-005), Google.org, the Oxford Martin School Programmes in Pandemic Genomics & Digital Pandemic Preparedness, European Union's Horizon Europe programme projects MOOD (#874850) and E4Warning (#101086640), Wellcome Trust grants 303666/Z/23/Z, 226052/Z/22/Z & 228186/Z/23/Z, the United Kingdom Research and Innovation (#APP8583), the Medical Research Foundation (MRF-RG-ICCH-2022-100069), UK International Development (301542-403), the Bill & Melinda Gates Foundation (INV-063472) and Novo Nordisk Foundation (NNF24OC0094346). The content and findings reported herein are the sole deduction, view and responsibility of the researcher/s and do not necessarily reflect the official position and sentiments of the funding agencies.

Funding Statement

The funders had no role in data collection, analysis, interpretation of data, writing of the manuscript, or the decision to submit it for publication.

5. References

1. Castilletti C, Mori A, Matucci A, et al. Oropouche fever cases diagnosed in Italy in two epidemiologically non-related travellers from Cuba, late May to early June 2024. *Eurosurveillance*. 2024;29(26):2400362. doi:10.2807/1560-7917.ES.2024.29.26.2400362

2. Sakkas H, Bozidis P, Franks A, Papadopoulou C. Oropouche Fever: A Review. *Viruses*. 2018;10(4):175. doi:10.3390/v10040175

3. Feitoza LHM, de Carvalho LPC, da Silva LR, et al. Influence of meteorological and seasonal parameters on the activity of Culicoides paraensis (Diptera: ceratopogonidae), an annoying anthropophilic biting midge and putative vector of Oropouche Virus in Rondônia, Brazilian Amazon. *Acta Trop*. 2023;243:106928.

4. Benitez AJ, Alvarez M, Perez L, et al. Oropouche Fever, Cuba, May 2024. *Emerg Infect Dis*. 2024;30(10):2155.

5. de Mendonça SF, Rocha MN, Ferreira FV, et al. Evaluation of Aedes aegypti, Aedes albopictus, and Culex quinquefasciatus Mosquitoes Competence to Oropouche virus Infection. *Viruses*. 2021;13(5):755. doi:10.3390/v13050755

6. Gutierrez B, Wise E, Pullan S, et al. The evolutionary dynamics of Oropouche virus (OROV) in South America. *bioRxiv*. Published online 2019:682559.

7. Hoch AL, Pinheiro F de P, Roberts DR, Gomez M de LC. Laboratory transmission of Oropouche virus by Culex quinquefasciatus Say. *Bull Pan Am Health Organ PAHO 21 1 1987*. Published online 1987.

8. Romero-Alvarez D, Escobar LE. Oropouche fever, an emergent disease from the Americas. *Microbes Infect*. 2018;20(3):135-146. doi:10.1016/j.micinf.2017.11.013

9. Gräf T, Delatorre E, do Nascimento Ferreira C, et al. Expansion of Oropouche virus in non-endemic Brazilian regions: analysis of genomic characterisation and ecological drivers. *Lancet Infect Dis*. Published online 2024.

10. Iani FC de M, Mota Pereira F, de Oliveira EC, et al. Rapid viral expansion beyond the Amazon Basin: increased epidemic activity of Oropouche virus across the Americas. *MedRxiv*. Published online 2024:2024-08.

11. Tegally H, Dellicour S, Poongavanan J, et al. Dynamics and ecology of a multi-stage expansion of Oropouche virus in Brazil. *medRxiv*. Published online 2024:2024-10.

12. PAHO. PAHO. Pan American Health Organization (PAHO). December 2, 2025. https://www.paho.org/es/arbo-portal/oropouche

13. LeDuc J, Hoch A, Pinheiro F de P, Da Rosa A. Epidemic Oropouche virus disease in northern Brazil. *Bull Pan Am Health Organ PAHO 15 2 1981*. Published online 1981.

14. Scachetti GC, Forato J, Claro IM, et al. Reemergence of Oropouche virus between 2023 and 2024 in Brazil. Published online July 30, 2024:2024.07.27.24310296. doi:10.1101/2024.07.27.24310296

15. Bandeira AC, Barbosa ACFN da S, Souza M, et al. Clinical profile of Oropouche fever in Bahia, Brazil: unexpected fatal cases. Published online 2024.

16. Singleton AL, Glidden CK, Chamberlin AJ, et al. Species distribution modeling for disease ecology: A multi-scale case study for schistosomiasis host snails in Brazil. *PLOS Glob Public Health*. 2024;4(8):e0002224. doi:10.1371/journal.pgph.0002224

17. Klitting R, Kafetzopoulou LE, Thiery W, et al. Predicting the evolution of the Lassa virus endemic area and population at risk over the next decades. *Nat Commun*. 2022;13(1):5596. doi:10.1038/s41467-022-33112-3

18. Escobar LE. Ecological niche modeling: an introduction for veterinarians and epidemiologists. *Front Vet Sci*. 2020;7:519059.

19. Barbet‐Massin M, Jiguet F, Albert CH, Thuiller W. Selecting pseudo‐absences for species distribution models: How, where and how many? *Methods Ecol Evol*. 2012;3(2):327-338.

20. Iturbide M, Bedia J, Herrera S, Hierro OD, Pinto M, Gutiérrez JM. A framework for species distribution modelling with improved pseudo-absence generation. *Ecol Model*. 2015;312. doi:10.1016/j.ecolmodel.2015.05.018

21. Yusuf IS, Tessera K ab, Tumiel T, et al. On pseudo-absence generation and machine learning for locust breeding ground prediction in Africa. Published online May 20, 2022. doi:10.48550/arXiv.2111.03904

22. Wisz MS, Guisan A. Do pseudo-absence selection strategies influence species distribution models and their predictions? An information-theoretic approach based on simulated data. *BMC Ecol*. 2009;9(1):8. doi:10.1186/1472-6785-9-8

23. Alaniz AJ, Carvajal MA, Bacigalupo A, Cattan PE. Global spatial assessment of Aedes aegypti and Culex quinquefasciatus: a scenario of Zika virus exposure. *Epidemiol Infect*. 2019;147:e52.

24. Carlson CJ, Albery GF, Merow C, et al. Climate change increases cross-species viral transmission risk. *Nature*. 2022;607(7919):555-562.

25. Peterson AT. *Mapping Disease Transmission Risk: Enriching Models Using Biogeography and Ecology*. JHU Press; 2014.

26. Ranc N, Santini L, Rondinini C, et al. Performance tradeoffs in target‐group bias correction for species distribution models. *Ecography*. 2017;40(9):1076-1087.

27. Milanesi P, Della Rocca F, Robinson RA. Integrating dynamic environmental predictors and species occurrences: Toward true dynamic species distribution models. *Ecol Evol*. 2020;10(2):1087-1092. doi:10.1002/ece3.5938

28. Lobo JM, Jiménez-Valverde A, Hortal J. The uncertain nature of absences and their importance in species distribution modelling. *Ecography*. 2010;33(1):103-114. doi:10.1111/j.1600-0587.2009.06039.x

29. Hazen EL, Abrahms B, Brodie S, Carroll G, Welch H, Bograd SJ. Where did they not go? Considerations for generating pseudo-absences for telemetry-based habitat models. *Mov Ecol*. 2021;9(1):5. doi:10.1186/s40462-021-00240-2

30. Liu C, Newell G, White M. The effect of sample size on the accuracy of species distribution models: considering both presences and pseudo-absences or background sites. *Ecography*. 2019;42(3):535-548. doi:10.1111/ecog.03188

31. Harrup L, Purse B, Golding N, Mellor P, Carpenter S. Larval development and emergence sites of farm‐associated Culicoides in the United Kingdom. *Med Vet Entomol*. 2013;27(4):441-449.

32. Carpenter S, Groschup MH, Garros C, Felippe-Bauer ML, Purse BV. Culicoides biting midges, arboviruses and public health in Europe. *Antiviral Res*. 2013;100(1):102-113.

33. Mordecai EA, Cohen JM, Evans MV, et al. Detecting the impact of temperature on transmission of Zika, dengue, and chikungunya using mechanistic models. *PLoS Negl Trop Dis*. 2017;11(4):e0005568. doi:10.1371/journal.pntd.0005568

34. Tilston-Lunel NL, Hughes J, Acrani GO, et al. Genetic analysis of members of the species Oropouche virus and identification of a novel M segment sequence. *J Gen Virol*. 2015;96(Pt_7):1636-1650.

35. Merow C, Smith MJ, Silander Jr JA. A practical guide to MaxEnt for modeling species' distributions: what it does, and why inputs and settings matter. *Ecography*. 2013;36(10):1058-1069.

36. Elith J, Graham CH. Do they? How do they? WHY do they differ? On finding reasons for differing performances of species distribution models. *Ecography*. 2009;32(1):66-77.

37. Valavi R, Guillera-Arroita G, Lahoz-Monfort JJ, Elith J. Predictive performance of presence-only species distribution models: a benchmark study with reproducible code. *Ecol Monogr*. 2022;92(1):e01486. doi:10.1002/ecm.1486

38. Breiman L. Random forests. *Mach Learn*. 2001;45:5-32.

39. Cutler DR, Edwards Jr TC, Beard KH, et al. Random forests for classification in ecology. *Ecology*. 2007;88(11):2783-2792.

40. Franklin J. *Mapping Species Distributions: Spatial Inference and Prediction*. Cambridge University Press; 2009.

41. Biau G, Scornet E. A random forest guided tour. *Test*. 2016;25:197-227.

42. Hertzog LR, Besnard A, Jay‐Robert P. Field validation shows bias‐corrected pseudo‐absence selection is the best method for predictive species‐distribution modelling. *Divers Distrib*. 2014;20(12):1403-1413.

43. Kramer-Schadt S, Niedballa J, Pilgrim JD, et al. The importance of correcting for sampling bias in MaxEnt species distribution models. *Divers Distrib*. 2013;19(11):1366-1379. doi:10.1111/ddi.12096

44. Phillips SJ, Dudík M, Elith J, et al. Sample selection bias and presence-only distribution models: implications for background and pseudo-absence data. *Ecol Appl*. 2009;19(1):181-197. doi:10.1890/07-2153.1

45. Brady O, Lim A, Shearer F, et al. The overlapping global distribution of dengue, chikungunya, Zika and yellow fever. Published online 2024.

46. Lorenz C, Azevedo TS, Virginio F, Aguiar BS, Chiaravalloti-Neto F, Suesdek L. Impact of environmental factors on neglected emerging arboviral diseases. *PLoS Negl Trop Dis*. 2017;11(9):e0005959.

47. Boyce MS, Vernier PR, Nielsen SE, Schmiegelow FKA. Evaluating resource selection functions.

Ecol Model. 2002;157(2):281-300. doi:10.1016/S0304-3800(02)00200-4

48. Hirzel AH, Le Lay G, Helfer V, Randin C, Guisan A. Evaluating the ability of habitat suitability models to predict species presences. *Ecol Model*. 2006;199(2):142-152. doi:10.1016/j.ecolmodel.2006.05.017

49. Breiner FT, Guisan A, Bergamini A, Nobis MP. Overcoming limitations of modelling rare species by using ensembles of small models. *Methods Ecol Evol*. 2015;6(10):1210-1218. doi:10.1111/2041-210X.12403

50. Muscarella R, Galante PJ, Soley‐Guardia M, et al. ENM eval: An R package for conducting spatially independent evaluations and estimating optimal model complexity for Maxent ecological niche models. *Methods Ecol Evol*. 2014;5(11):1198-1205.

51. Araújo MB, New M. Ensemble forecasting of species distributions. *Trends Ecol Evol*. 2007;22(1):42-47.

52. Marmion M, Parviainen M, Luoto M, Heikkinen RK, Thuiller W. Evaluation of consensus methods in predictive species distribution modelling. *Divers Distrib*. 2009;15(1):59-69. doi:10.1111/j.1472-4642.2008.00491.x

53. de Sousa Farias E, Júnior AMP, Almeida JF, Pessoa FAC, Medeiros JF. Hematophagous biting midges (Diptera: Ceratopogonidae) from Tefé municipality, Amazonas state, Brazil. *Check List*. 2015;11(4):1676-1676.

54. Felippe-Bauer ML, Gonzaga GP, Cavalcante RC, Gomes RG, Silva RA. Culicoides (Diptera: Ceratopogonidae) from Ceará State, northeastern Brazil: Diversity, new records and bionomic approaches. *Cuad Investig UNED*. 2019;11(2):137-144.

55. Walsh CES, Robert MA, Christofferson RC. Observational Characterization of the Ecological and Environmental Features Associated with the Presence of Oropouche Virus and the Primary Vector Culicoides paraensis: Data Synthesis and Systematic Review. *Trop Med Infect Dis*. 2021;6(3):143. doi:10.3390/tropicalmed6030143

6. Supplementary Materials

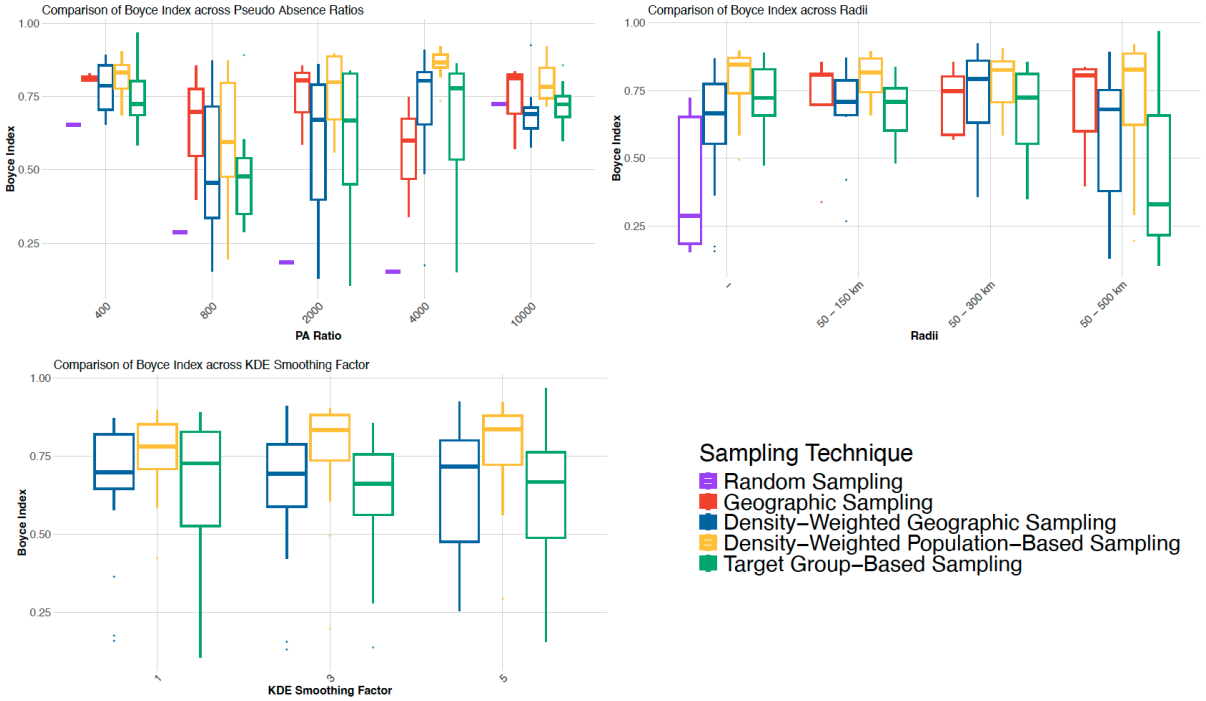

Figure S1 Comparison of Boyce Index across different pseudo-absence sampling strategies, evaluated using (A) pseudo-absence ratios, (B) geographic buffer radii, and (C) kernel density estimation (KDE) smoothing factors. The boxplots display the distribution of Boyce Index values for each sampling strategy, with higher values indicating better model performance. Sampling techniques include Random Sampling (purple), Geographic Sampling (red), Density-Weighted Geographic Sampling (blue), Density-Weighted Population-Based Sampling (yellow), and Target Group-Based Sampling (green).

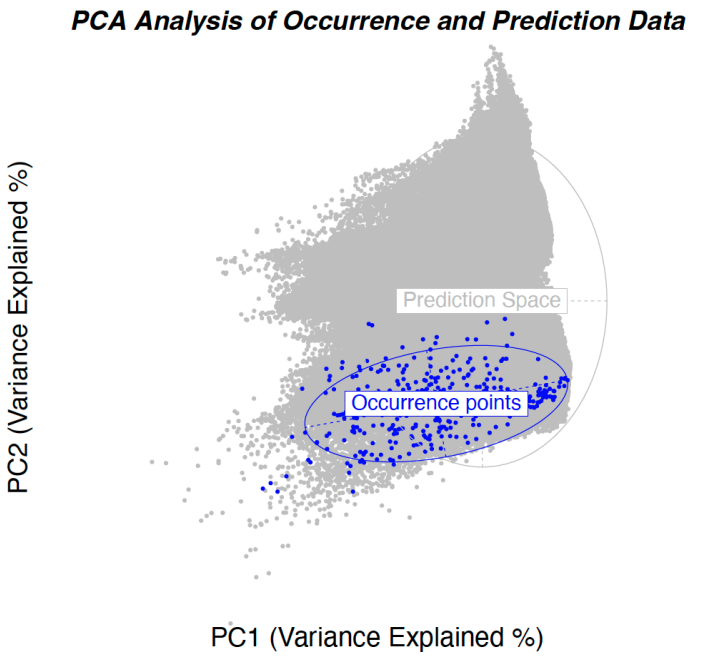

Figure S2 Principal Component Analysis (PCA) comparing environmental conditions in the occurrence points (blue) and the prediction space (grey). The PCA was conducted using the 26 environmental variables included in the model. The blue ellipse highlights the environmental conditions associated with observed occurrences, while the grey background represents the broader environmental space where predictions were made.

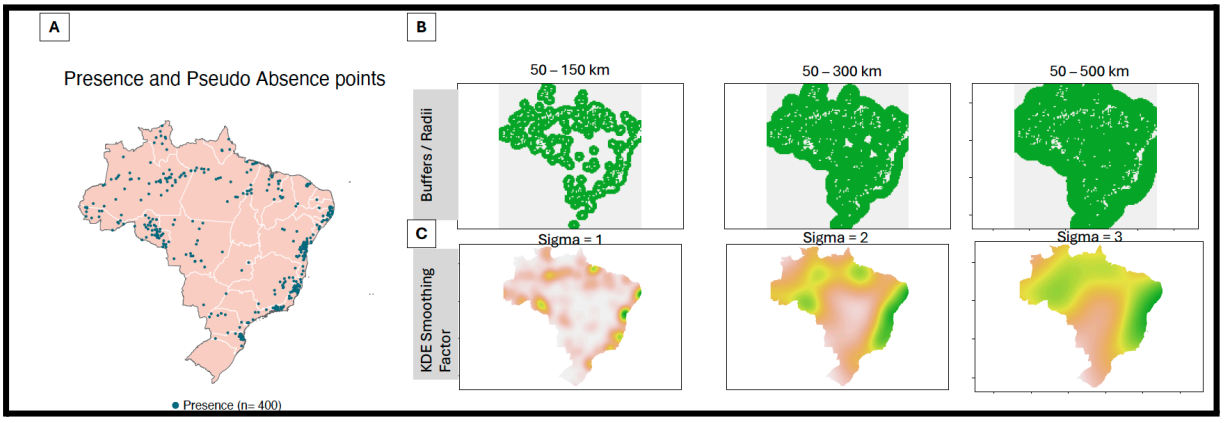

Figure S3 Illustration of spatial distribution of presence and pseudo-absence points used for modeling. (A) Map of 400 presence points (blue) distributed across Brazil. (B) Pseudo-absence selection using geographic buffers around presence points, with three buffer radii: 50–150 km, 50–300 km, and 50–500 km. Increasing the buffer size results in a broader spatial distribution of pseudo-absence points (green). (C) Kernel Density Estimation (KDE) smoothing factors (σ = 1, 2, 3) used to weight pseudo-absence selection based on occurrence point density. Higher σ values result in more spatially generalized pseudo-absence distributions. [Please not this is for illustration purposes].

		Pseudo-Absence Sampling Techniques				
		Random Sampling	Geographic Sampling	Density_weighted Geographic Sampling	Density-Weighted Population-Based Sampling	Target Group-Based Sampling
Constraint/ Parameters	PA Ratio	x5	x5	x5	x5	x5
	Buffer	N/A	x3	x4	x4	x4
	KDE SF	N/A	N/A	x3	x3	x3
Numbre of Models generated for each pseudo-absence sampling technique		5	15	60	60	60

Figure S4 Summary of the number of models generated under each pseudo-absence sampling technique. Models were generated based on combinations of pseudo-absence (PA) ratios, geographic buffer radii, and Kernel Density Estimation (KDE) smoothing factors (σ). The table shows how different factors were applied across five sampling techniques: Random Sampling, Geographic Sampling, Density-Weighted Geographic Sampling, Density-Weighted Population-Based Sampling, and Target Group-Based Sampling. The final number of models reflects the total combinations of PA ratio, buffer size, and KDE smoothing factor used for each method.

Table S1: Environmental variables used in the study with respective description and data sources.

	Environmental Variables	**Description**	**Source**
1.	Elevation	Height above sea level	USGS
2.	Herbaceous vegetation area	Land covered predominantly by grass and non-woody plants	MODIS Land Cover, Global Land Cover (GLC)
3.	Cultivated managed vegetation area	Irrigated croplands / managed terrestrial vegetation	EarthEnv - https://www.earthenv.org/landcover

4.	Regularly flooded vegetation area	Areas of vegetation subject to periodic or continuous flooding	EarthEnv - https://www.earthenv.org/landcover
5.	Deciduous broadleaf forest area	Forests dominated by broadleaf trees that shed leaves seasonally	EarthEnv - https://www.earthenv.org/landcover
6.	Evergreen broadleaf forest area	Forests dominated by broadleaf trees that retain foliage year-round	EarthEnv - https://www.earthenv.org/landcover
7.	Grasslands area	Open landscapes dominated by grasses with little to no tree cover	EarthEnv - https://www.earthenv.org/landcover
8.	Shrublands area	Land dominated by shrubs and low woody vegetation	EarthEnv - https://www.earthenv.org/landcover
9.	Savannas area	Tropical ecosystem characterised by grasses interspersed with scattered trees and shrubs	EarthEnv: https://www.earthenv.org/landcover
10.	Woody savannas area	Savannas with a higher density of trees	EarthEnv - https://www.earthenv.org/landcover
11.	Natural vegetation area	Areas dominated by native vegetation, excluding managed or cultivated lands	EarthEnv - https://www.earthenv.org/landcover
12.	Cropland area	Areas predominantly used for growing crops	EarthEnv - https://www.earthenv.org/landcover
13.	Banana harvested area	Land used for cultivating bananas	EarthEnv - https://www.earthenv.org/landcover

14.	Cassava harvested area	Land used for cultivating cassava (a root crop)	EarthEnv - https://www.earthenv.org/landcover
15.	Cocoa harvested area	Land used for cultivating cocoa trees	EarthEnv - https://www.earthenv.org/landcover
16.	Coffee harvested area	Land used for cultivating coffee plants	EarthEnv - https://www.earthenv.org/landcover
17.	Maize harvested area	Land used for growing maize (corn)	EarthEnv - https://www.earthenv.org/landcover
18.	Soybean harvested area	Land used for cultivating soybeans	EarthEnv - https://www.earthenv.org/landcover
19.	Sugarcane harvested area	Land used for cultivating sugarcane	EarthEnv - https://www.earthenv.org/landcover
20.	Cattle cultivation area	Areas designated for cattle farming and grazing	EarthEnv - https://www.earthenv.org/landcover
21.	Forest loss (2020-2023)	Areas of forest cover lost due to deforestation, logging, or natural events	https://glad.earthengine.app/view/global-forest-change
22.	Water occurrence	The presence and distribution of surface water bodies over time	Global surface water explorer
23.	Minimum and Maximum Temperature	Minimum and Maximum annual mean Temperature	https://cds.climate.copernicus.eu/datasets
24.	Temperature	Mean Annual Temperature	https://cds.climate.copernicus.eu/datasets

25.	Soil Moisture	Content of liquid water in a surface soil layer of 2 to 5 cm depth expressed as the percentage of total saturation.	https://cds.climate.copernicus.eu/datasets
26.	Humidity	Amount of water vapour in the air, measured as a %.	https://cds.climate.copernicus.eu/datasets

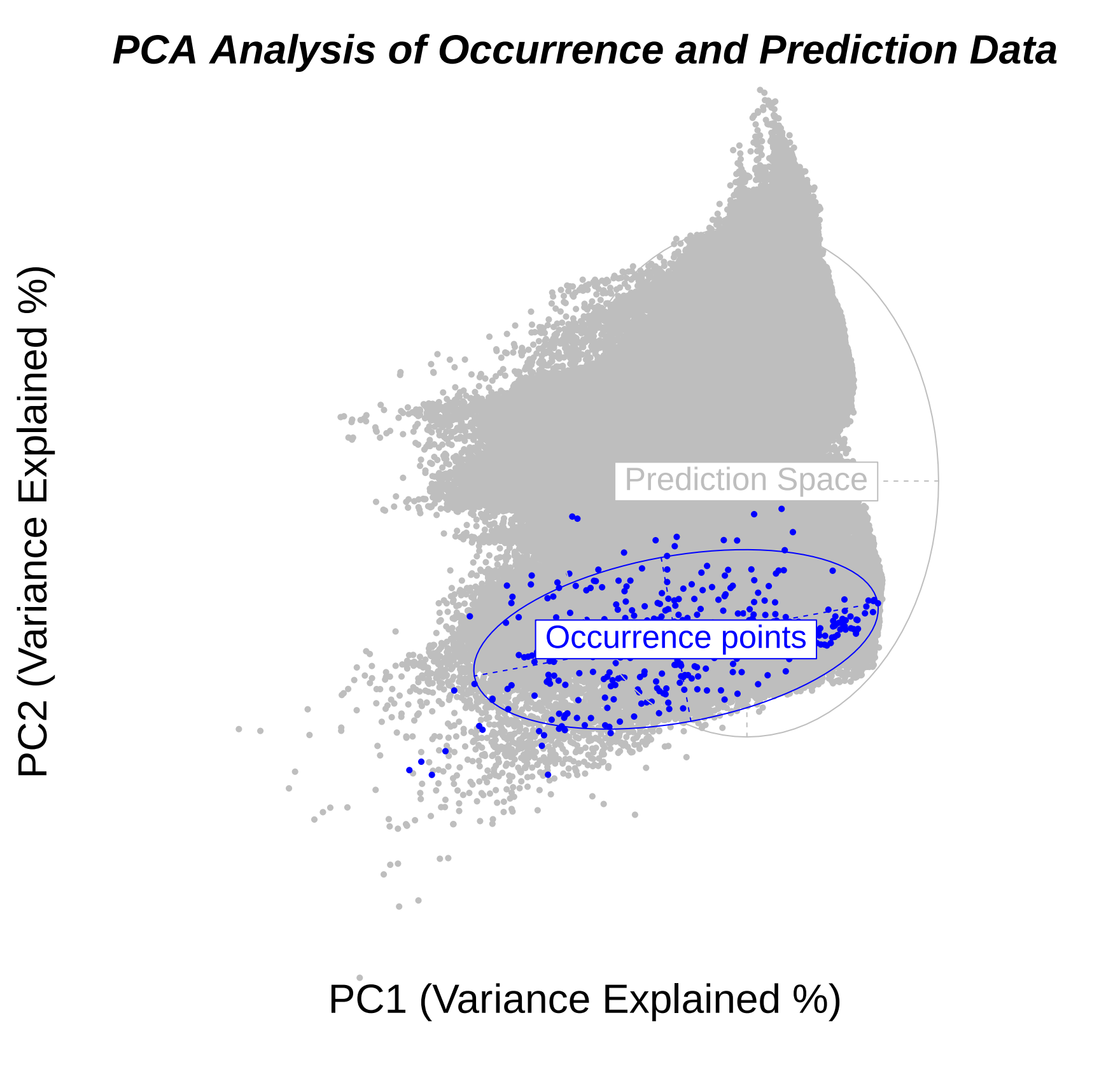
PCA Analysis of Occurrence and Prediction Data
PC2 (Variance Explained %)
PC1 (Variance Explained %)
Prediction Space
Occurrence points

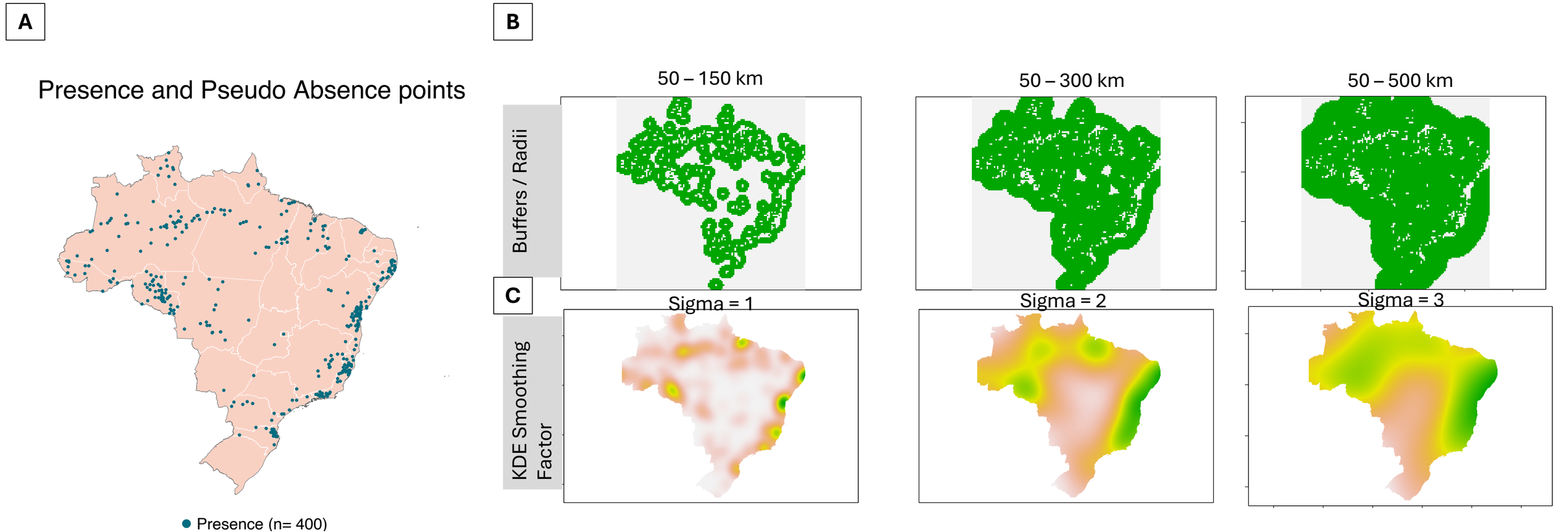
A
Presence and Pseudo Absence points
Presence (n= 400)
B
50 – 150 km
50 – 300 km
50 – 500 km
Buffers / Radii
C
KDE Smoothing Factor
Sigma = 1
Sigma = 2
Sigma = 3

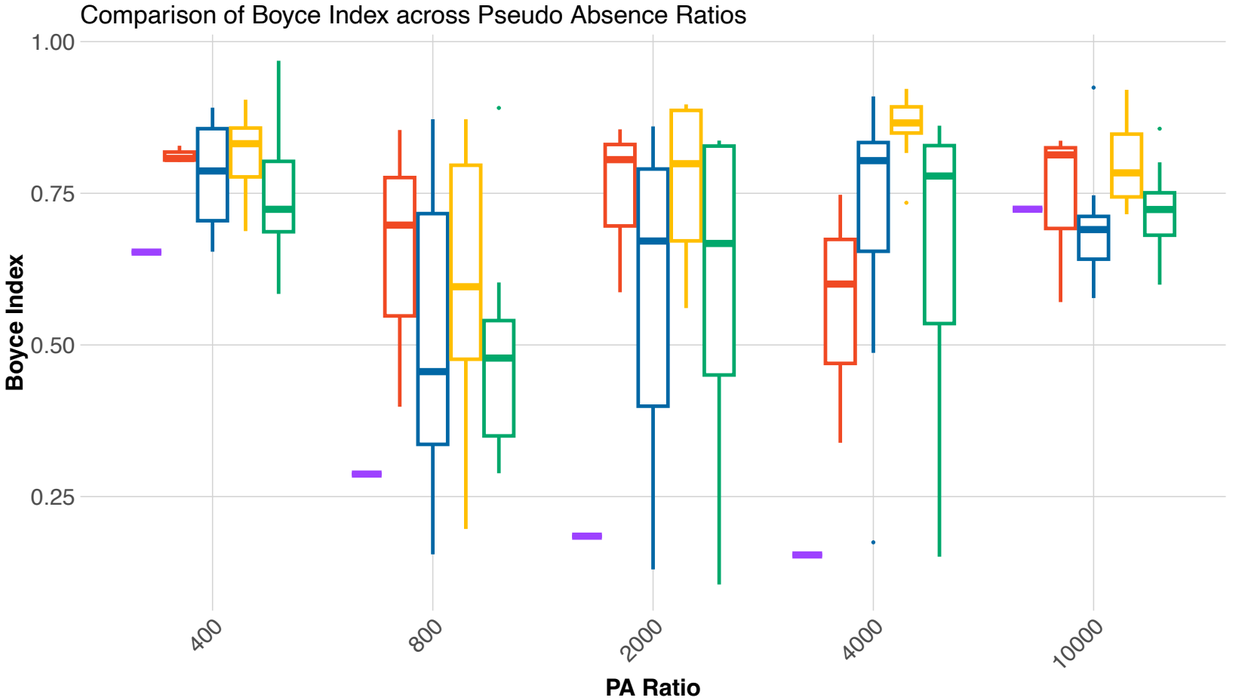
Comparison of Boyce Index across Pseudo Absence Ratios
Boyce Index
1.00
0.75
0.50
0.25
400
800
2000
4000
10000
PA Ratio

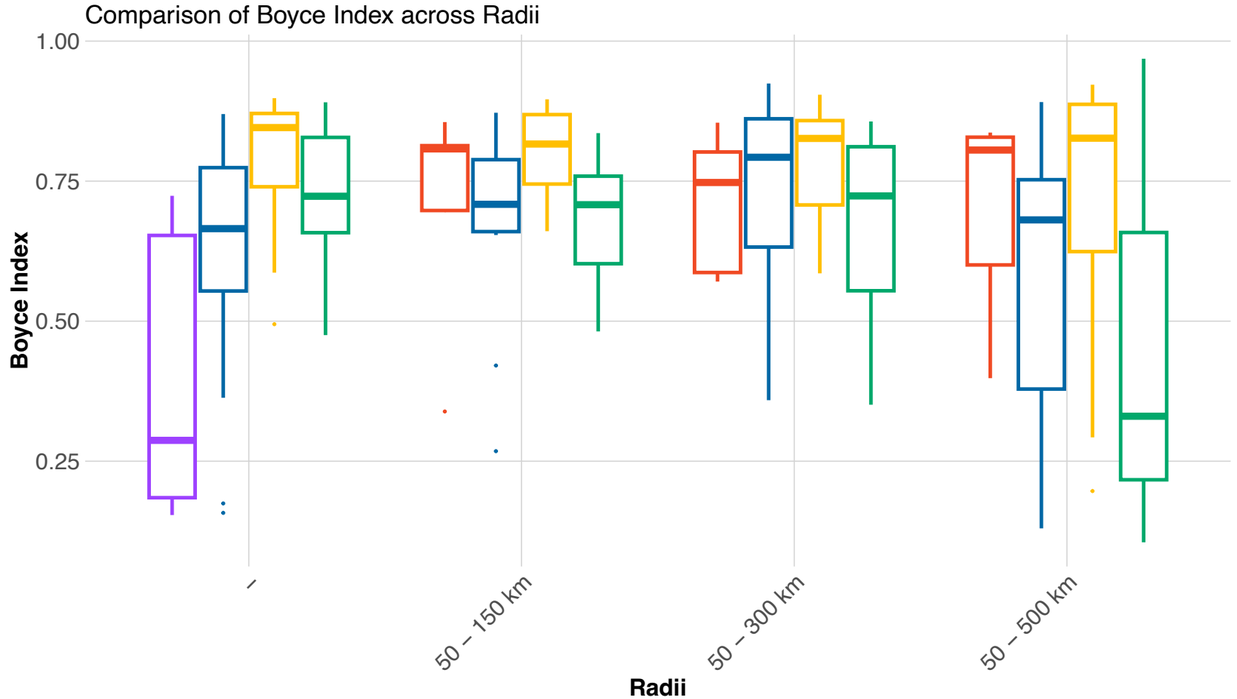
Comparison of Boyce Index across Radii
Boyce Index
1.00
0.75
0.50
0.25
–
50 – 150 km
50 – 300 km
50 – 500 km
Radii

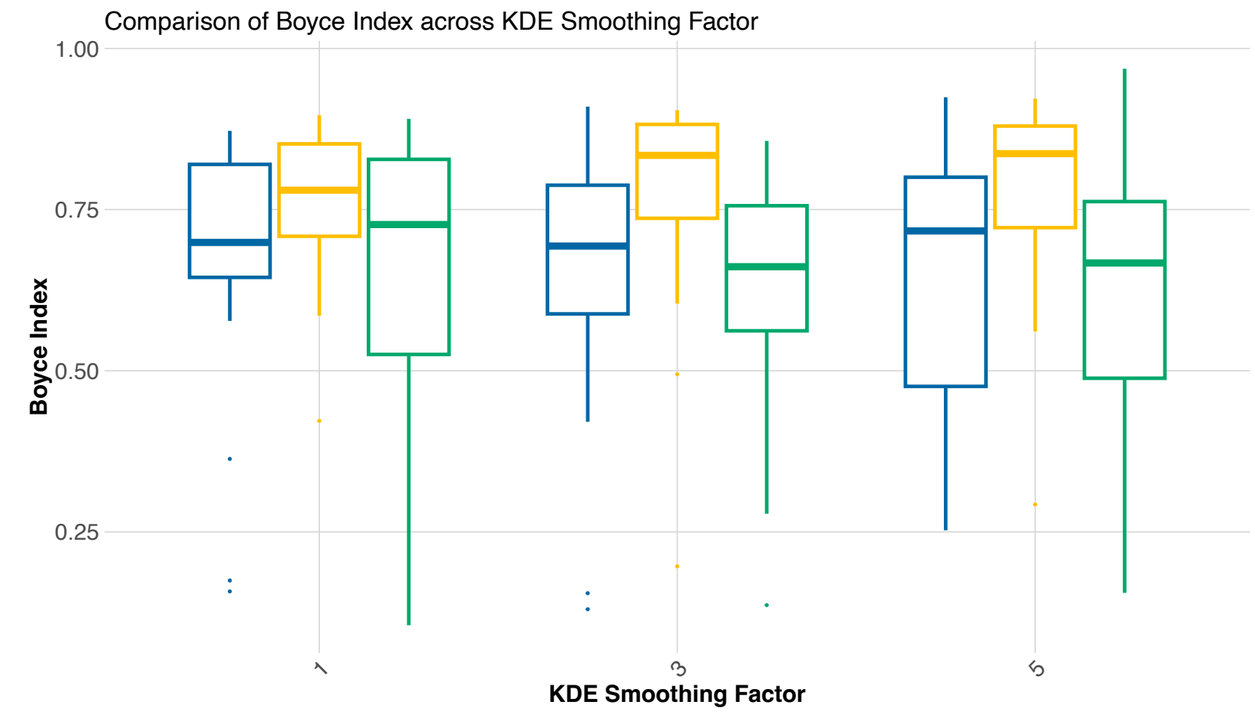
Comparison of Boyce Index across KDE Smoothing Factor
Boyce Index
1.00
0.75
0.50
0.25
1
3
5
KDE Smoothing Factor

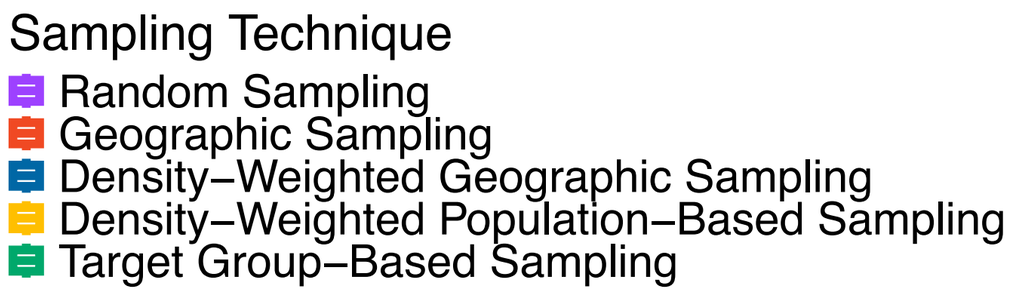
Sampling Technique
Random Sampling
Geographic Sampling
Density–Weighted Geographic Sampling
Density–Weighted Population–Based Sampling
Target Group–Based Sampling

Table S1: Environmental variables used in the study with respective description and data sources.

	Environmental Variables	**Description**	**Source**
1.	Elevation	Height above sea level	USGS
2.	Herbaceous vegetation area	Land covered predominantly by grass and non-woody plants	MODIS Land Cover, Global Land Cover (GLC)
3.	Cultivated managed vegetation area	Irrigated croplands / managed terrestrial vegetation	EarthEnv - https://www.earthenv.org/landcover
4.	Regularly flooded vegetation area	Areas of vegetation subject to periodic or continuous flooding	EarthEnv - https://www.earthenv.org/landcover
5.	Deciduous broadleaf forest area	Forests dominated by broadleaf trees that shed leaves seasonally	EarthEnv - https://www.earthenv.org/landcover
6.	Evergreen broadleaf forest area	Forests dominated by broadleaf trees that retain foliage year-round	EarthEnv - https://www.earthenv.org/landcover
7.	Grasslands area	Open landscapes dominated by grasses with little to no tree cover	EarthEnv - https://www.earthenv.org/landcover
8.	Shrublands area	Land dominated by shrubs and low woody vegetation	EarthEnv - https://www.earthenv.org/landcover
9.	Savannas area	Tropical ecosystem characterised by grasses interspersed with scattered trees and shrubs	EarthEnv: https://www.earthenv.org/landcover

10.	Woody savannas area	Savannas with a higher density of trees	EarthEnv - https://www.earthenv.org/landcover
11.	Natural vegetation area	Areas dominated by native vegetation, excluding managed or cultivated lands	EarthEnv - https://www.earthenv.org/landcover
12.	Cropland area	Areas predominantly used for growing crops	EarthEnv - https://www.earthenv.org/landcover
13.	Banana harvested area	Land used for cultivating bananas	EarthEnv - https://www.earthenv.org/landcover
14.	Cassava harvested area	Land used for cultivating cassava (a root crop)	EarthEnv - https://www.earthenv.org/landcover
15.	Cocoa harvested area	Land used for cultivating cocoa trees	EarthEnv - https://www.earthenv.org/landcover
16.	Coffee harvested area	Land used for cultivating coffee plants	EarthEnv - https://www.earthenv.org/landcover
17.	Maize harvested area	Land used for growing maize (corn)	EarthEnv - https://www.earthenv.org/landcover
18.	Soybean harvested area	Land used for cultivating soybeans	EarthEnv - https://www.earthenv.org/landcover
19.	Sugarcane harvested area	Land used for cultivating sugarcane	EarthEnv - https://www.earthenv.org/landcover

20.	Cattle cultivation area	Areas designated for cattle farming and grazing	EarthEnv - https://www.earthenv.org/landcover
21.	Forest loss (2020-2023)	Areas of forest cover lost due to deforestation, logging, or natural events	https://glad.earthengine.app/view/global-forest-change
22.	Water occurrence	The presence and distribution of surface water bodies over time	Global surface water explorer
23.	Minimum and Maximum Temperature	Minimum and Maximum annual mean Temperature	https://cds.climate.copernicus.eu/datasets
24.	Temperature	Mean Annual Temperature	https://cds.climate.copernicus.eu/datasets
25.	Soil Moisture	Content of liquid water in a surface soil layer of 2 to 5 cm depth expressed as the percentage of total saturation.	https://cds.climate.copernicus.eu/datasets
26.	Humidity	Amount of water vapour in the air, measured as a %.	https://cds.climate.copernicus.eu/datasets

Sampling Technique	Sigma	Radii	PA Ratio	Evaluation Metric	MeanVal	min	max
Target Group Based Approach	1	0	400	ROC	0.81566667	0.776	0.945
Target Group Based Approach	1	0	400	TSS	0.46266667	0.258	0.568
Target Group Based Approach	1	0	800	ROC	0.81316667	0.774	0.904
Target Group Based Approach	1	0	800	TSS	0.50241667	0.399	0.656
Target Group Based Approach	1	0	2000	ROC	0.79525	0.745	0.866
Target Group Based Approach	1	0	2000	TSS	0.4215	0.176	0.611
Target Group Based Approach	1	0	4000	ROC	0.78883333	0.728	0.873
Target Group Based Approach	1	0	4000	TSS	0.35666667	0.163	0.583
Target Group Based Approach	1	0	10000	ROC	0.76416667	0.644	0.851
Target Group Based Approach	1	0	10000	TSS	0.23675	0.109	0.437
Target Group Based Approach	1	50-150 km	400	ROC	0.85133333	0.747	0.949
Target Group Based Approach	1	50-150 km	400	TSS	0.47183333	0.132	0.805
Target Group Based Approach	1	50-150 km	800	ROC	0.85916667	0.778	0.933
Target Group Based Approach	1	50-150 km	800	TSS	0.52458333	0.216	0.842
Target Group Based Approach	1	50-150 km	2000	ROC	0.85125	0.745	0.939
Target Group Based Approach	1	50-150 km	2000	TSS	0.44858333	0.129	0.726
Target Group Based Approach	1	50-150 km	4000	ROC	0.83175	0.69	0.939
Target Group Based Approach	1	50-150 km	4000	TSS	0.4225	0.086	0.666
Target Group Based Approach	1	50-150 km	10000	ROC	0.81191667	0.633	0.91
Target Group Based Approach	1	50-150 km	10000	TSS	0.38633333	0.084	0.63
Target Group Based Approach	1	50-300 km	400	ROC	0.86583333	0.801	0.944
Target Group Based Approach	1	50-300 km	400	TSS	0.555	0.281	0.745
Target Group Based Approach	1	50-300 km	800	ROC	0.87783333	0.798	0.95
Target Group Based Approach	1	50-300 km	800	TSS	0.56741667	0.303	0.758
Target Group Based Approach	1	50-300 km	2000	ROC	0.86008333	0.769	0.946
Target Group Based Approach	1	50-300 km	2000	TSS	0.49191667	0.243	0.726
Target Group Based Approach	1	50-300 km	4000	ROC	0.85058333	0.762	0.918

Target Group Based Approach	1	50-300 km	4000	TSS	0.46141667	0.23	0.66
Target Group Based Approach	1	50-300 km	10000	ROC	0.82491667	0.693	0.906
Target Group Based Approach	1	50-300 km	10000	TSS	0.4085	0.125	0.648
Target Group Based Approach	1	50-500km	400	ROC	0.85383333	0.775	0.97
Target Group Based Approach	1	50-500km	400	TSS	0.55333333	0.244	0.791
Target Group Based Approach	1	50-500km	800	ROC	0.87425	0.784	0.945
Target Group Based Approach	1	50-500km	800	TSS	0.59783333	0.326	0.793
Target Group Based Approach	1	50-500km	2000	ROC	0.86866667	0.792	0.922
Target Group Based Approach	1	50-500km	2000	TSS	0.53508333	0.343	0.782
Target Group Based Approach	1	50-500km	4000	ROC	0.85616667	0.763	0.925
Target Group Based Approach	1	50-500km	4000	TSS	0.49875	0.266	0.688
Target Group Based Approach	1	50-500km	10000	ROC	0.8435	0.728	0.931
Target Group Based Approach	1	50-500km	10000	TSS	0.42516667	0.158	0.649
Target Group Based Approach	3	0	400	ROC	0.84283333	0.79	0.932
Target Group Based Approach	3	0	400	TSS	0.55375	0.356	0.839
Target Group Based Approach	3	0	800	ROC	0.827	0.762	0.928
Target Group Based Approach	3	0	800	TSS	0.49991667	0.33	0.775
Target Group Based Approach	3	0	2000	ROC	0.82475	0.767	0.906
Target Group Based Approach	3	0	2000	TSS	0.44558333	0.261	0.736
Target Group Based Approach	3	0	4000	ROC	0.82333333	0.77	0.93
Target Group Based Approach	3	0	4000	TSS	0.44333333	0.195	0.652
Target Group Based Approach	3	0	10000	ROC	0.80025	0.704	0.899
Target Group Based Approach	3	0	10000	TSS	0.29983333	0.103	0.446
Target Group Based Approach	3	50-150 km	400	ROC	0.875	0.756	0.96
Target Group Based Approach	3	50-150 km	400	TSS	0.47316667	0.114	0.843
Target Group Based Approach	3	50-150 km	800	ROC	0.86875	0.775	0.965
Target Group Based Approach	3	50-150 km	800	TSS	0.54575	0.289	0.742
Target Group Based Approach	3	50-150 km	2000	ROC	0.85591667	0.721	0.95

Target Group Based Approach	3	50-150 km	2000	TSS	0.47375	0.121	0.783
Target Group Based Approach	3	50-150 km	4000	ROC	0.83483333	0.685	0.948
Target Group Based Approach	3	50-150 km	4000	TSS	0.431	0.14	0.651
Target Group Based Approach	3	50-150 km	10000	ROC	0.81483333	0.647	0.924
Target Group Based Approach	3	50-150 km	10000	TSS	0.37741667	0.107	0.625
Target Group Based Approach	3	50-300 km	400	ROC	0.865	0.79	0.965
Target Group Based Approach	3	50-300 km	400	TSS	0.53333333	0.266	0.883
Target Group Based Approach	3	50-300 km	800	ROC	0.89433333	0.811	0.956
Target Group Based Approach	3	50-300 km	800	TSS	0.62283333	0.38	0.851
Target Group Based Approach	3	50-300 km	2000	ROC	0.88075	0.8	0.95
Target Group Based Approach	3	50-300 km	2000	TSS	0.558	0.226	0.838
Target Group Based Approach	3	50-300 km	4000	ROC	0.8715	0.792	0.944
Target Group Based Approach	3	50-300 km	4000	TSS	0.51558333	0.308	0.651
Target Group Based Approach	3	50-300 km	10000	ROC	0.855	0.739	0.935
Target Group Based Approach	3	50-300 km	10000	TSS	0.45741667	0.197	0.69
Target Group Based Approach	3	50-500km	400	ROC	0.88675	0.808	0.976
Target Group Based Approach	3	50-500km	400	TSS	0.61833333	0.339	0.945
Target Group Based Approach	3	50-500km	800	ROC	0.89408333	0.827	0.953
Target Group Based Approach	3	50-500km	800	TSS	0.65025	0.433	0.846
Target Group Based Approach	3	50-500km	2000	ROC	0.88141667	0.804	0.937
Target Group Based Approach	3	50-500km	2000	TSS	0.59983333	0.459	0.777
Target Group Based Approach	3	50-500km	4000	ROC	0.87533333	0.797	0.944
Target Group Based Approach	3	50-500km	4000	TSS	0.51741667	0.294	0.715
Target Group Based Approach	3	50-500km	10000	ROC	0.85516667	0.753	0.933
Target Group Based Approach	3	50-500km	10000	TSS	0.46808333	0.253	0.679
Target Group Based Approach	5	0	400	ROC	0.82175	0.729	0.915
Target Group Based Approach	5	0	400	TSS	0.48766667	0.229	0.684
Target Group Based Approach	5	0	800	ROC	0.84475	0.791	0.94

Target Group Based Approach	5	0	800	TSS	0.53408333	0.274	0.777
Target Group Based Approach	5	0	2000	ROC	0.84233333	0.777	0.925
Target Group Based Approach	5	0	2000	TSS	0.50608333	0.157	0.734
Target Group Based Approach	5	0	4000	ROC	0.82225	0.76	0.91
Target Group Based Approach	5	0	4000	TSS	0.40441667	0.157	0.508
Target Group Based Approach	5	0	10000	ROC	0.80525	0.717	0.904
Target Group Based Approach	5	0	10000	TSS	0.25516667	0.097	0.498
Target Group Based Approach	5	50-150 km	400	ROC	0.857	0.749	0.953
Target Group Based Approach	5	50-150 km	400	TSS	0.51458333	0.088	0.802
Target Group Based Approach	5	50-150 km	800	ROC	0.87308333	0.773	0.958
Target Group Based Approach	5	50-150 km	800	TSS	0.5565	0.273	0.812
Target Group Based Approach	5	50-150 km	2000	ROC	0.85225	0.739	0.947
Target Group Based Approach	5	50-150 km	2000	TSS	0.45758333	0.164	0.741
Target Group Based Approach	5	50-150 km	4000	ROC	0.82841667	0.675	0.928
Target Group Based Approach	5	50-150 km	4000	TSS	0.42708333	0.11	0.635
Target Group Based Approach	5	50-150 km	10000	ROC	0.80291667	0.605	0.909
Target Group Based Approach	5	50-150 km	10000	TSS	0.38066667	0.076	0.623
Target Group Based Approach	5	50-300 km	400	ROC	0.886	0.81	0.963
Target Group Based Approach	5	50-300 km	400	TSS	0.59466667	0.466	0.843
Target Group Based Approach	5	50-300 km	800	ROC	0.89283333	0.824	0.959
Target Group Based Approach	5	50-300 km	800	TSS	0.61566667	0.422	0.826
Target Group Based Approach	5	50-300 km	2000	ROC	0.88375	0.807	0.944
Target Group Based Approach	5	50-300 km	2000	TSS	0.56283333	0.286	0.767
Target Group Based Approach	5	50-300 km	4000	ROC	0.869	0.796	0.948
Target Group Based Approach	5	50-300 km	4000	TSS	0.52241667	0.27	0.675
Target Group Based Approach	5	50-300 km	10000	ROC	0.85341667	0.747	0.931
Target Group Based Approach	5	50-300 km	10000	TSS	0.47825	0.257	0.673
Target Group Based Approach	5	50-500km	400	ROC	0.90183333	0.843	0.965

Target Group Based Approach		5	50-500km	400	TSS	0.74558333	0.669	0.809
Target Group Based Approach		5	50-500km	800	ROC	0.90575	0.836	0.961
Target Group Based Approach		5	50-500km	800	TSS	0.64725	0.506	0.782
Target Group Based Approach		5	50-500km	2000	ROC	0.88466667	0.822	0.952
Target Group Based Approach		5	50-500km	2000	TSS	0.56675	0.323	0.81
Target Group Based Approach		5	50-500km	4000	ROC	0.88483333	0.808	0.953
Target Group Based Approach		5	50-500km	4000	TSS	0.568	0.349	0.668
Target Group Based Approach		5	50-500km	10000	ROC	0.85741667	0.77	0.937
Target Group Based Approach		5	50-500km	10000	TSS	0.48116667	0.286	0.655
Random Sampling	-	-		400	ROC	0.83891667	0.73	0.938
Random Sampling	-	-		400	TSS	0.49783333	0.164	0.76
Random Sampling	-	-		800	ROC	0.85275	0.78	0.94
Random Sampling	-	-		800	TSS	0.53791667	0.412	0.741
Random Sampling	-	-		2000	ROC	0.83916667	0.745	0.925
Random Sampling	-	-		2000	TSS	0.45583333	0.161	0.59
Random Sampling	-	-		4000	ROC	0.82141667	0.746	0.907
Random Sampling	-	-		4000	TSS	0.33258333	0.159	0.532
Random Sampling	-	-		10000	ROC	0.60366667	0.509	0.749
Random Sampling	-	-		10000	TSS	0.258	0.042	0.506
Density-Weighted Population-Based Approach		1	0	400	ROC	0.68191667	0.646	0.731
Density-Weighted Population-Based Approach		1	0	400	TSS	0.25916667	0.187	0.354
Density-Weighted Population-Based Approach		1	0	800	ROC	0.66991667	0.545	0.81
Density-Weighted Population-Based Approach		1	0	800	TSS	0.21641667	0.081	0.422
Density-Weighted Population-Based Approach		1	0	2000	ROC	0.65533333	0.574	0.773
Density-Weighted Population-Based Approach		1	0	2000	TSS	0.19383333	0.058	0.386
Density-Weighted Population-Based Approach		1	0	4000	ROC	0.64641667	0.513	0.765
Density-Weighted Population-Based Approach		1	0	4000	TSS	0.14716667	0.004	0.277
Density-Weighted Population-Based Approach		1	0	10000	ROC	0.63666667	0.473	0.797

Density-Weighted Population-Based Approach	1	0	10000	TSS	0.07491667	-0.031	0.158
Density-Weighted Population-Based Approach	1	50-150 km	400	ROC	0.80625	0.682	0.933
Density-Weighted Population-Based Approach	1	50-150 km	400	TSS	0.35825	0.159	0.661
Density-Weighted Population-Based Approach	1	50-150 km	800	ROC	0.80758333	0.692	0.928
Density-Weighted Population-Based Approach	1	50-150 km	800	TSS	0.38525	0.163	0.715
Density-Weighted Population-Based Approach	1	50-150 km	2000	ROC	0.79133333	0.634	0.905
Density-Weighted Population-Based Approach	1	50-150 km	2000	TSS	0.37491667	0.135	0.658
Density-Weighted Population-Based Approach	1	50-150 km	4000	ROC	0.76583333	0.598	0.877
Density-Weighted Population-Based Approach	1	50-150 km	4000	TSS	0.34575	0.088	0.61
Density-Weighted Population-Based Approach	1	50-150 km	10000	ROC	0.74	0.56	0.856
Density-Weighted Population-Based Approach	1	50-150 km	10000	TSS	0.28975	0.059	0.596
Density-Weighted Population-Based Approach	1	50-300 km	400	ROC	0.82458333	0.753	0.94
Density-Weighted Population-Based Approach	1	50-300 km	400	TSS	0.4405	0.247	0.707
Density-Weighted Population-Based Approach	1	50-300 km	800	ROC	0.82083333	0.686	0.923
Density-Weighted Population-Based Approach	1	50-300 km	800	TSS	0.40083333	0.138	0.703
Density-Weighted Population-Based Approach	1	50-300 km	2000	ROC	0.79616667	0.632	0.907
Density-Weighted Population-Based Approach	1	50-300 km	2000	TSS	0.38441667	0.152	0.667
Density-Weighted Population-Based Approach	1	50-300 km	4000	ROC	0.76858333	0.601	0.862
Density-Weighted Population-Based Approach	1	50-300 km	4000	TSS	0.34841667	0.097	0.565
Density-Weighted Population-Based Approach	1	50-300 km	10000	ROC	0.7505	0.565	0.888
Density-Weighted Population-Based Approach	1	50-300 km	10000	TSS	0.30608333	0.079	0.607
Density-Weighted Population-Based Approach	1	50-500km	400	ROC	0.80275	0.699	0.894
Density-Weighted Population-Based Approach	1	50-500km	400	TSS	0.38258333	0.223	0.673
Density-Weighted Population-Based Approach	1	50-500km	800	ROC	0.82233333	0.715	0.915
Density-Weighted Population-Based Approach	1	50-500km	800	TSS	0.45408333	0.194	0.729
Density-Weighted Population-Based Approach	1	50-500km	2000	ROC	0.79425	0.638	0.905
Density-Weighted Population-Based Approach	1	50-500km	2000	TSS	0.38333333	0.097	0.702
Density-Weighted Population-Based Approach	1	50-500km	4000	ROC	0.76833333	0.607	0.882

Density-Weighted Population-Based Approach	1	50-500km	4000	TSS	0.35575	0.088	0.627
Density-Weighted Population-Based Approach	1	50-500km	10000	ROC	0.7495	0.56	0.871
Density-Weighted Population-Based Approach	1	50-500km	10000	TSS	0.29958333	0.082	0.61
Density-Weighted Population-Based Approach	3	0	400	ROC	0.742	0.686	0.796
Density-Weighted Population-Based Approach	3	0	400	TSS	0.33333333	0.184	0.486
Density-Weighted Population-Based Approach	3	0	800	ROC	0.76625	0.722	0.837
Density-Weighted Population-Based Approach	3	0	800	TSS	0.384	0.259	0.579
Density-Weighted Population-Based Approach	3	0	2000	ROC	0.735	0.689	0.767
Density-Weighted Population-Based Approach	3	0	2000	TSS	0.3145	0.216	0.434
Density-Weighted Population-Based Approach	3	0	4000	ROC	0.72425	0.621	0.783
Density-Weighted Population-Based Approach	3	0	4000	TSS	0.22966667	0.132	0.367
Density-Weighted Population-Based Approach	3	0	10000	ROC	0.69191667	0.564	0.761
Density-Weighted Population-Based Approach	3	0	10000	TSS	0.13783333	-0.003	0.3
Density-Weighted Population-Based Approach	3	50-150 km	400	ROC	0.8165	0.733	0.923
Density-Weighted Population-Based Approach	3	50-150 km	400	TSS	0.44475	0.223	0.753
Density-Weighted Population-Based Approach	3	50-150 km	800	ROC	0.82091667	0.723	0.913
Density-Weighted Population-Based Approach	3	50-150 km	800	TSS	0.44283333	0.16	0.686
Density-Weighted Population-Based Approach	3	50-150 km	2000	ROC	0.8115	0.68	0.895
Density-Weighted Population-Based Approach	3	50-150 km	2000	TSS	0.38183333	0.181	0.657
Density-Weighted Population-Based Approach	3	50-150 km	4000	ROC	0.79358333	0.63	0.891
Density-Weighted Population-Based Approach	3	50-150 km	4000	TSS	0.37791667	0.128	0.633
Density-Weighted Population-Based Approach	3	50-150 km	10000	ROC	0.76358333	0.586	0.878
Density-Weighted Population-Based Approach	3	50-150 km	10000	TSS	0.32858333	0.117	0.618
Density-Weighted Population-Based Approach	3	50-300 km	400	ROC	0.84641667	0.76	0.935
Density-Weighted Population-Based Approach	3	50-300 km	400	TSS	0.52808333	0.415	0.711
Density-Weighted Population-Based Approach	3	50-300 km	800	ROC	0.84608333	0.782	0.916
Density-Weighted Population-Based Approach	3	50-300 km	800	TSS	0.4905	0.234	0.721
Density-Weighted Population-Based Approach	3	50-300 km	2000	ROC	0.8315	0.731	0.907

Density-Weighted Population-Based Approach	3	50-300 km	2000	TSS	0.42158333	0.118	0.64
Density-Weighted Population-Based Approach	3	50-300 km	4000	ROC	0.81625	0.692	0.906
Density-Weighted Population-Based Approach	3	50-300 km	4000	TSS	0.41941667	0.146	0.623
Density-Weighted Population-Based Approach	3	50-300 km	10000	ROC	0.80225	0.647	0.903
Density-Weighted Population-Based Approach	3	50-300 km	10000	TSS	0.36783333	0.139	0.62
Density-Weighted Population-Based Approach	3	50-500km	400	ROC	0.83275	0.746	0.934
Density-Weighted Population-Based Approach	3	50-500km	400	TSS	0.42858333	-0.011	0.664
Density-Weighted Population-Based Approach	3	50-500km	800	ROC	0.85808333	0.771	0.937
Density-Weighted Population-Based Approach	3	50-500km	800	TSS	0.51675	0.335	0.746
Density-Weighted Population-Based Approach	3	50-500km	2000	ROC	0.84141667	0.763	0.909
Density-Weighted Population-Based Approach	3	50-500km	2000	TSS	0.48041667	0.268	0.655
Density-Weighted Population-Based Approach	3	50-500km	4000	ROC	0.82058333	0.712	0.903
Density-Weighted Population-Based Approach	3	50-500km	4000	TSS	0.42483333	0.22	0.647
Density-Weighted Population-Based Approach	3	50-500km	10000	ROC	0.80408333	0.655	0.893
Density-Weighted Population-Based Approach	3	50-500km	10000	TSS	0.3845	0.169	0.641
Density-Weighted Population-Based Approach	5	0	400	ROC	0.768	0.731	0.842
Density-Weighted Population-Based Approach	5	0	400	TSS	0.36758333	0.172	0.511
Density-Weighted Population-Based Approach	5	0	800	ROC	0.74591667	0.538	0.799
Density-Weighted Population-Based Approach	5	0	800	TSS	0.33016667	0.083	0.465
Density-Weighted Population-Based Approach	5	0	2000	ROC	0.73875	0.696	0.77
Density-Weighted Population-Based Approach	5	0	2000	TSS	0.28641667	0.034	0.451
Density-Weighted Population-Based Approach	5	0	4000	ROC	0.7325	0.699	0.809
Density-Weighted Population-Based Approach	5	0	4000	TSS	0.24175	0.168	0.335
Density-Weighted Population-Based Approach	5	0	10000	ROC	0.70475	0.575	0.779
Density-Weighted Population-Based Approach	5	0	10000	TSS	0.13766667	-0.002	0.239
Density-Weighted Population-Based Approach	5	50-150 km	400	ROC	0.84541667	0.741	0.946
Density-Weighted Population-Based Approach	5	50-150 km	400	TSS	0.49325	0.241	0.714
Density-Weighted Population-Based Approach	5	50-150 km	800	ROC	0.82441667	0.715	0.908

Density-Weighted Population-Based Approach	5	50-150 km	800	TSS	0.42675	0.208	0.662
Density-Weighted Population-Based Approach	5	50-150 km	2000	ROC	0.81075	0.663	0.92
Density-Weighted Population-Based Approach	5	50-150 km	2000	TSS	0.37975	0.145	0.657
Density-Weighted Population-Based Approach	5	50-150 km	4000	ROC	0.79508333	0.638	0.888
Density-Weighted Population-Based Approach	5	50-150 km	4000	TSS	0.37558333	0.114	0.611
Density-Weighted Population-Based Approach	5	50-150 km	10000	ROC	0.76958333	0.591	0.872
Density-Weighted Population-Based Approach	5	50-150 km	10000	TSS	0.31175	0.083	0.603
Density-Weighted Population-Based Approach	5	50-300 km	400	ROC	0.85366667	0.785	0.974
Density-Weighted Population-Based Approach	5	50-300 km	400	TSS	0.49291667	0.247	0.706
Density-Weighted Population-Based Approach	5	50-300 km	800	ROC	0.8565	0.795	0.931
Density-Weighted Population-Based Approach	5	50-300 km	800	TSS	0.46483333	0.206	0.693
Density-Weighted Population-Based Approach	5	50-300 km	2000	ROC	0.85066667	0.755	0.934
Density-Weighted Population-Based Approach	5	50-300 km	2000	TSS	0.46325	0.21	0.727
Density-Weighted Population-Based Approach	5	50-300 km	4000	ROC	0.827	0.71	0.905
Density-Weighted Population-Based Approach	5	50-300 km	4000	TSS	0.42975	0.25	0.61
Density-Weighted Population-Based Approach	5	50-300 km	10000	ROC	0.8045	0.671	0.897
Density-Weighted Population-Based Approach	5	50-300 km	10000	TSS	0.38708333	0.171	0.619
Density-Weighted Population-Based Approach	5	50-500km	400	ROC	0.8745	0.797	0.967
Density-Weighted Population-Based Approach	5	50-500km	400	TSS	0.52566667	0	0.82
Density-Weighted Population-Based Approach	5	50-500km	800	ROC	0.8555	0.779	0.931
Density-Weighted Population-Based Approach	5	50-500km	800	TSS	0.53033333	0.192	0.673
Density-Weighted Population-Based Approach	5	50-500km	2000	ROC	0.84908333	0.768	0.917
Density-Weighted Population-Based Approach	5	50-500km	2000	TSS	0.49391667	0.327	0.676
Density-Weighted Population-Based Approach	5	50-500km	4000	ROC	0.83075	0.723	0.916
Density-Weighted Population-Based Approach	5	50-500km	4000	TSS	0.45958333	0.21	0.668
Density-Weighted Population-Based Approach	5	50-500km	10000	ROC	0.81166667	0.691	0.906
Density-Weighted Population-Based Approach	5	50-500km	10000	TSS	0.38325	0.18	0.632
Density-Weighted Geographic Sampling	1	0	400	ROC	0.76175	0.645	0.917

Density-Weighted Geographic Sampling	1	0	400	TSS	0.40183333	0.088	0.721
Density-Weighted Geographic Sampling	1	0	800	ROC	0.76241667	0.681	0.898
Density-Weighted Geographic Sampling	1	0	800	TSS	0.33225	0.116	0.651
Density-Weighted Geographic Sampling	1	0	2000	ROC	0.73933333	0.638	0.871
Density-Weighted Geographic Sampling	1	0	2000	TSS	0.27591667	0.114	0.545
Density-Weighted Geographic Sampling	1	0	4000	ROC	0.71016667	0.575	0.874
Density-Weighted Geographic Sampling	1	0	4000	TSS	0.17225	0	0.426
Density-Weighted Geographic Sampling	1	0	10000	ROC	0.69741667	0.529	0.877
Density-Weighted Geographic Sampling	1	0	10000	TSS	0.1275	0	0.39
Density-Weighted Geographic Sampling	1	50-150 km	400	ROC	0.84716667	0.762	0.954
Density-Weighted Geographic Sampling	1	50-150 km	400	TSS	0.46925	0.127	0.828
Density-Weighted Geographic Sampling	1	50-150 km	800	ROC	0.85091667	0.773	0.944
Density-Weighted Geographic Sampling	1	50-150 km	800	TSS	0.51066667	0.262	0.808
Density-Weighted Geographic Sampling	1	50-150 km	2000	ROC	0.84283333	0.734	0.946
Density-Weighted Geographic Sampling	1	50-150 km	2000	TSS	0.44825	0.194	0.71
Density-Weighted Geographic Sampling	1	50-150 km	4000	ROC	0.81641667	0.694	0.938
Density-Weighted Geographic Sampling	1	50-150 km	4000	TSS	0.42758333	0.169	0.592
Density-Weighted Geographic Sampling	1	50-150 km	10000	ROC	0.79641667	0.658	0.931
Density-Weighted Geographic Sampling	1	50-150 km	10000	TSS	0.34383333	0.106	0.565
Density-Weighted Geographic Sampling	1	50-300 km	400	ROC	0.86016667	0.782	0.952
Density-Weighted Geographic Sampling	1	50-300 km	400	TSS	0.53266667	0.217	0.808
Density-Weighted Geographic Sampling	1	50-300 km	800	ROC	0.86116667	0.792	0.948
Density-Weighted Geographic Sampling	1	50-300 km	800	TSS	0.53508333	0.306	0.78
Density-Weighted Geographic Sampling	1	50-300 km	2000	ROC	0.83525	0.727	0.937
Density-Weighted Geographic Sampling	1	50-300 km	2000	TSS	0.46216667	0.194	0.622
Density-Weighted Geographic Sampling	1	50-300 km	4000	ROC	0.82825	0.683	0.931
Density-Weighted Geographic Sampling	1	50-300 km	4000	TSS	0.41791667	0.179	0.609
Density-Weighted Geographic Sampling	1	50-300 km	10000	ROC	0.81158333	0.681	0.923

Density-Weighted Geographic Sampling	1	50-300 km	10000	TSS	0.36433333	0.154	0.594
Density-Weighted Geographic Sampling	1	50-500km	400	ROC	0.85116667	0.79	0.95
Density-Weighted Geographic Sampling	1	50-500km	400	TSS	0.49383333	0.181	0.831
Density-Weighted Geographic Sampling	1	50-500km	800	ROC	0.85083333	0.759	0.944
Density-Weighted Geographic Sampling	1	50-500km	800	TSS	0.50466667	0.299	0.826
Density-Weighted Geographic Sampling	1	50-500km	2000	ROC	0.85191667	0.757	0.948
Density-Weighted Geographic Sampling	1	50-500km	2000	TSS	0.48	0.144	0.727
Density-Weighted Geographic Sampling	1	50-500km	4000	ROC	0.82541667	0.688	0.941
Density-Weighted Geographic Sampling	1	50-500km	4000	TSS	0.41783333	0.133	0.584
Density-Weighted Geographic Sampling	1	50-500km	10000	ROC	0.80475	0.689	0.915
Density-Weighted Geographic Sampling	1	50-500km	10000	TSS	0.34291667	0.153	0.573
Density-Weighted Geographic Sampling	3	0	400	ROC	0.84225	0.751	0.934
Density-Weighted Geographic Sampling	3	0	400	TSS	0.51466667	0.245	0.797
Density-Weighted Geographic Sampling	3	0	800	ROC	0.84141667	0.794	0.918
Density-Weighted Geographic Sampling	3	0	800	TSS	0.49383333	0.43	0.67
Density-Weighted Geographic Sampling	3	0	2000	ROC	0.816	0.744	0.923
Density-Weighted Geographic Sampling	3	0	2000	TSS	0.34641667	0.198	0.562
Density-Weighted Geographic Sampling	3	0	4000	ROC	0.81191667	0.68	0.92
Density-Weighted Geographic Sampling	3	0	4000	TSS	0.35516667	0.216	0.518
Density-Weighted Geographic Sampling	3	0	10000	ROC	0.786	0.641	0.911
Density-Weighted Geographic Sampling	3	0	10000	TSS	0.23675	0.011	0.443
Density-Weighted Geographic Sampling	3	50-150 km	400	ROC	0.8705	0.796	0.958
Density-Weighted Geographic Sampling	3	50-150 km	400	TSS	0.57458333	0.3	0.863
Density-Weighted Geographic Sampling	3	50-150 km	800	ROC	0.87033333	0.783	0.948
Density-Weighted Geographic Sampling	3	50-150 km	800	TSS	0.55383333	0.294	0.83
Density-Weighted Geographic Sampling	3	50-150 km	2000	ROC	0.85991667	0.755	0.949
Density-Weighted Geographic Sampling	3	50-150 km	2000	TSS	0.51383333	0.256	0.691
Density-Weighted Geographic Sampling	3	50-150 km	4000	ROC	0.834	0.69	0.938

Density-Weighted Geographic Sampling	3	50-150 km	4000	TSS	0.46308333	0.221	0.651
Density-Weighted Geographic Sampling	3	50-150 km	10000	ROC	0.808	0.647	0.923
Density-Weighted Geographic Sampling	3	50-150 km	10000	TSS	0.37875	0.175	0.614
Density-Weighted Geographic Sampling	3	50-300 km	400	ROC	0.894	0.813	0.959
Density-Weighted Geographic Sampling	3	50-300 km	400	TSS	0.604	0.411	0.897
Density-Weighted Geographic Sampling	3	50-300 km	800	ROC	0.88991667	0.819	0.949
Density-Weighted Geographic Sampling	3	50-300 km	800	TSS	0.60325	0.326	0.809
Density-Weighted Geographic Sampling	3	50-300 km	2000	ROC	0.878	0.795	0.946
Density-Weighted Geographic Sampling	3	50-300 km	2000	TSS	0.53166667	0.28	0.701
Density-Weighted Geographic Sampling	3	50-300 km	4000	ROC	0.86433333	0.768	0.945
Density-Weighted Geographic Sampling	3	50-300 km	4000	TSS	0.49975	0.296	0.683
Density-Weighted Geographic Sampling	3	50-300 km	10000	ROC	0.84858333	0.723	0.93
Density-Weighted Geographic Sampling	3	50-300 km	10000	TSS	0.45266667	0.241	0.667
Density-Weighted Geographic Sampling	3	50-500km	400	ROC	0.88866667	0.79	0.96
Density-Weighted Geographic Sampling	3	50-500km	400	TSS	0.61925	0.381	0.868
Density-Weighted Geographic Sampling	3	50-500km	800	ROC	0.88975	0.834	0.956
Density-Weighted Geographic Sampling	3	50-500km	800	TSS	0.59225	0.237	0.859
Density-Weighted Geographic Sampling	3	50-500km	2000	ROC	0.8885	0.813	0.943
Density-Weighted Geographic Sampling	3	50-500km	2000	TSS	0.58408333	0.411	0.706
Density-Weighted Geographic Sampling	3	50-500km	4000	ROC	0.86858333	0.781	0.945
Density-Weighted Geographic Sampling	3	50-500km	4000	TSS	0.50483333	0.281	0.686
Density-Weighted Geographic Sampling	3	50-500km	10000	ROC	0.84775	0.726	0.924
Density-Weighted Geographic Sampling	3	50-500km	10000	TSS	0.46241667	0.25	0.663
Density-Weighted Geographic Sampling	5	0	400	ROC	0.83225	0.699	0.95
Density-Weighted Geographic Sampling	5	0	400	TSS	0.52033333	0.15	0.87
Density-Weighted Geographic Sampling	5	0	800	ROC	0.83508333	0.745	0.929
Density-Weighted Geographic Sampling	5	0	800	TSS	0.47041667	0.24	0.785
Density-Weighted Geographic Sampling	5	0	2000	ROC	0.84066667	0.783	0.921

Density-Weighted Geographic Sampling	5	0	2000	TSS	0.4215	0.212	0.61
Density-Weighted Geographic Sampling	5	0	4000	ROC	0.83091667	0.73	0.932
Density-Weighted Geographic Sampling	5	0	4000	TSS	0.38	0.204	0.522
Density-Weighted Geographic Sampling	5	0	10000	ROC	0.79875	0.677	0.913
Density-Weighted Geographic Sampling	5	0	10000	TSS	0.27691667	0.019	0.426
Density-Weighted Geographic Sampling	5	50-150 km	400	ROC	0.87716667	0.803	0.944
Density-Weighted Geographic Sampling	5	50-150 km	400	TSS	0.56858333	0.212	0.821
Density-Weighted Geographic Sampling	5	50-150 km	800	ROC	0.86641667	0.741	0.956
Density-Weighted Geographic Sampling	5	50-150 km	800	TSS	0.561	0.248	0.844
Density-Weighted Geographic Sampling	5	50-150 km	2000	ROC	0.86108333	0.744	0.945
Density-Weighted Geographic Sampling	5	50-150 km	2000	TSS	0.51333333	0.265	0.694
Density-Weighted Geographic Sampling	5	50-150 km	4000	ROC	0.84408333	0.692	0.926
Density-Weighted Geographic Sampling	5	50-150 km	4000	TSS	0.46091667	0.233	0.648
Density-Weighted Geographic Sampling	5	50-150 km	10000	ROC	0.81266667	0.639	0.925
Density-Weighted Geographic Sampling	5	50-150 km	10000	TSS	0.36516667	0.162	0.595
Density-Weighted Geographic Sampling	5	50-300 km	400	ROC	0.88308333	0.813	0.958
Density-Weighted Geographic Sampling	5	50-300 km	400	TSS	0.59275	0.322	0.88
Density-Weighted Geographic Sampling	5	50-300 km	800	ROC	0.89941667	0.842	0.955
Density-Weighted Geographic Sampling	5	50-300 km	800	TSS	0.63316667	0.376	0.86
Density-Weighted Geographic Sampling	5	50-300 km	2000	ROC	0.89708333	0.827	0.945
Density-Weighted Geographic Sampling	5	50-300 km	2000	TSS	0.57616667	0.311	0.807
Density-Weighted Geographic Sampling	5	50-300 km	4000	ROC	0.87725	0.792	0.945
Density-Weighted Geographic Sampling	5	50-300 km	4000	TSS	0.52275	0.302	0.675
Density-Weighted Geographic Sampling	5	50-300 km	10000	ROC	0.84625	0.747	0.932
Density-Weighted Geographic Sampling	5	50-300 km	10000	TSS	0.44833333	0.229	0.668
Density-Weighted Geographic Sampling	5	50-500km	400	ROC	0.89908333	0.854	0.958
Density-Weighted Geographic Sampling	5	50-500km	400	TSS	0.65983333	0.524	0.895
Density-Weighted Geographic Sampling	5	50-500km	800	ROC	0.91216667	0.851	0.957

Density-Weighted Geographic Sampling		5	50-500km	800	TSS	0.65058333	0.436	0.804
Density-Weighted Geographic Sampling		5	50-500km	2000	ROC	0.9005	0.833	0.949
Density-Weighted Geographic Sampling		5	50-500km	2000	TSS	0.59883333	0.384	0.771
Density-Weighted Geographic Sampling		5	50-500km	4000	ROC	0.88141667	0.806	0.947
Density-Weighted Geographic Sampling		5	50-500km	4000	TSS	0.55691667	0.299	0.692
Density-Weighted Geographic Sampling		5	50-500km	10000	ROC	0.85833333	0.78	0.929
Density-Weighted Geographic Sampling		5	50-500km	10000	TSS	0.487	0.296	0.68
Geographic Sampling	-		50-150 km	400	ROC	0.86083333	0.775	0.952
Geographic Sampling	-		50-150 km	400	TSS	0.4555	0.127	0.789
Geographic Sampling	-		50-300 km	400	ROC	0.89233333	0.82	0.993
Geographic Sampling	-		50-300 km	400	TSS	0.57475	0.277	0.833
Geographic Sampling	-		50-500km	400	ROC	0.88041667	0.818	0.952
Geographic Sampling	-		50-500km	400	TSS	0.59375	0.373	0.852
Geographic Sampling	-		50-150 km	800	ROC	0.86725	0.79	0.955
Geographic Sampling	-		50-150 km	800	TSS	0.558	0.283	0.798
Geographic Sampling	-		50-300 km	800	ROC	0.8745	0.804	0.953
Geographic Sampling	-		50-300 km	800	TSS	0.55208333	0.239	0.811
Geographic Sampling	-		50-500km	800	ROC	0.8985	0.848	0.953
Geographic Sampling	-		50-500km	800	TSS	0.57658333	0.239	0.817
Geographic Sampling	-		50-150 km	2000	ROC	0.85041667	0.735	0.94
Geographic Sampling	-		50-150 km	2000	TSS	0.45075	0.231	0.601
Geographic Sampling	-		50-300 km	2000	ROC	0.88308333	0.817	0.965
Geographic Sampling	-		50-300 km	2000	TSS	0.54525	0.192	0.795
Geographic Sampling	-		50-500km	2000	ROC	0.89125	0.823	0.949
Geographic Sampling	-		50-500km	2000	TSS	0.55983333	0.399	0.686
Geographic Sampling	-		50-150 km	4000	ROC	0.83041667	0.719	0.926
Geographic Sampling	-		50-150 km	4000	TSS	0.42766667	0.21	0.587
Geographic Sampling	-		50-300 km	4000	ROC	0.8715	0.79	0.938

Geographic Sampling	-	50-300 km	4000	TSS	0.50258333	0.273	0.66
Geographic Sampling	-	50-500km	4000	ROC	0.87133333	0.814	0.935
Geographic Sampling	-	50-500km	4000	TSS	0.50591667	0.34	0.683
Geographic Sampling	-	50-150 km	10000	ROC	0.81025	0.681	0.91
Geographic Sampling	-	50-150 km	10000	TSS	0.34691667	0.118	0.594
Geographic Sampling	-	50-300 km	10000	ROC	0.84383333	0.757	0.914
Geographic Sampling	-	50-300 km	10000	TSS	0.41708333	0.175	0.655
Geographic Sampling	-	50-500km	10000	ROC	0.85983333	0.781	0.931
Geographic Sampling	-	50-500km	10000	TSS	0.43666667	0.196	0.66

		Pseudo-Absence Sampling Techniques				
		Random Sampling	**Geographic Sampling**	**Density-weighted Geographic Sampling**	**Density-Weighted Population-Based Sampling**	**Target Group-Based Sampling**
Constraint/ Parameters	**PA Ratio**	x5	x5	x5	x5	x5
	Buffer	N/A	x3	x4	x4	x4
	KDE SF	N/A	N/A	x3	x3	x3
Number of Models generated for each pseudo-absence sampling technique		5	15	60	60	60